

Methods for obtaining polarized xenon for magnetic resonance imaging. Review

© G.Y. Grigoriev, A.S. Lagutin

National Research Center „Kurchatov Institute“,
123182 Moscow, Russia
e-mail: lagutin_as@nrcki.ru

Received March 28, 2022

Revised May 18, 2022

Accepted May 18, 2022

A review of experimental studies and design developments of devices for obtaining nuclear-spin hyperpolarized ^{129}Xe by optical pumping of rubidium vapor with subsequent spin exchange with noble gas isotope atoms is presented. Hyperpolarized ^{129}Xe atom is an excellent probe in magnetic resonance imaging in studies of lung structure and function, and biomarkers based on it are applicable for the diagnosis of a wide range of both pulmonary and other diseases. The principles of operation, advantages and disadvantages of polarizer design options are outlined. The main attention is paid to new approaches and technical solutions that determine the trends in the development of the methodology.

Keywords: hyperpolarized xenon, lasers, optical pumping, nuclear magnetic resonance, magnetic resonance imaging.

DOI: 10.21883/TP.2022.09.54672.65-22

Introduction

The noble gas xenon attracts clinical researchers from all over the world since the 1940-s, and more than 20 years have passed since the official approval for the medical xenon use in Russia as an anesthetic [1]. Xenon is now recognized as the most safe anesthetic of the 21st century. Over 20 years of clinical use in Russia, more than 50 000 surgeries with the xenon use have been performed. The experience of application in anesthesiology made it possible not only to prove that xenon does not have even a minimum toxic effect on the human body and demonstrates cardio- and neuroprotective properties, but also has a wide range of therapeutic effects that can be used for therapeutic purposes in various areas of applied medicine: neurology, psychiatrics, addictology, cardiology, pulmonology, sports medicine, emergency medicine and disaster medicine [2]. However, this review deals with the production and use of the stable xenon isotope ^{129}Xe with nuclei hyperpolarized (HP) in magnetic moment as a contrast agent in functional magnetic resonance imaging (MRI). In MRI the phenomenon of nuclear magnetic resonance (NMR) is used. The important NMR parameter is the degree of polarization of nuclei P [3]

$$P = \frac{N_-}{N_+} = e^{-E/kT}.$$

Here, the minus and plus indices refer to different orientations of spins in a magnetic field, E is the energy of transition between these states, k is the Boltzmann constant, T is temperature. For protons at room temperature in a field of order 3 T the degree of polarization is approximately 10^{-5} . HP isotopes of noble gases (^3He , ^{129}Xe) have a degree of polarization close to 1 (at least $P \sim 20\text{--}70\%$),

which makes it possible to increase the contrast and resolution of MRI by several orders of magnitude.

Table 1 from the paper [4] presents comparative characteristics of parameters important for NMR. Despite the relatively low value of the gyromagnetic ratio, ^{129}Xe is a convenient contrast agent for MRI due to rather large chemical shift of NMR resonance lines in various media.

Methods for obtaining hyperpolarized nuclear spins in solids, liquids and gases are described in a number include of reviews and monographs [5–8], which the Brute–Force Hyperpolarization [9], spin exchange optical pumping (SEOP) [10], dynamic nuclear polarization (DNP) [11], chemically induced dynamic nuclear polarization (CIDNP) [12], photo -CIDNP [13], parahydrogen-induced polarization (PHIP) [14] and signal amplification by reversible exchange (SABRE) [15].

The most commonly used method for noble HP gases production is the method of optical pumping of alkali atoms followed by spin exchange with noble gas isotopes (spin-exchange optical pumping or SEOP). All subsequent developments of SEOP method are based on the pioneer researches of Ecole Normale Supérieure de Paris scientists in the late 40-x–early 50-s of the XX century [16–18]. In 1966 one of these scientists (Alfred Kastler) was awarded the Nobel Prize in physics for demonstrating that electronic spin order can be created in alkali metal vapors using circularly polarized light [19].

Let us review qualitatively the SEOP process, which consists of two stages, using the example of rubidium and xenon. At the first stage, optical pumping of vapors of the alkali atom occurs, the structure of its energy levels is shown in Fig. 1.

Table 1. Characteristics of nuclei used in MRI

Parameter	¹ H	³ He	¹²⁹ Xe
Natural prevalence, %	99.99	$1.37 \cdot 10^{-4}$	26.44
Nuclear spin	1/2	1/2	1/2
Gyromagnetic ratio, MHz/T	42.58	-32.43	-11.78
Spin density, 10^{19} atoms/cm ³	6690	2.37	2.37
Chemical shift range, ppm	~ 10	~ 0.8	~ 250

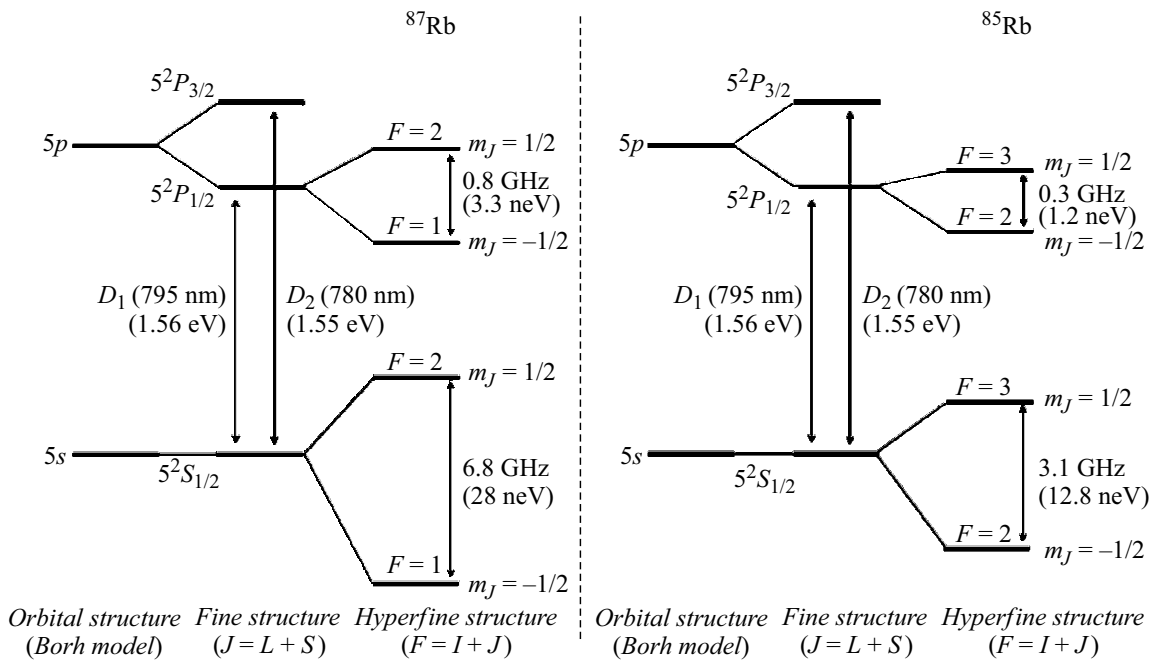


Figure 1. Structure of the levels of D-line of ⁸⁷Rb and ⁸⁵Rb used for optical pumping in the absence of the external magnetic field. The hyperfine splitting of the second perturbed level ⁵2P_{3/2} is not shown. Energy scale is not met.

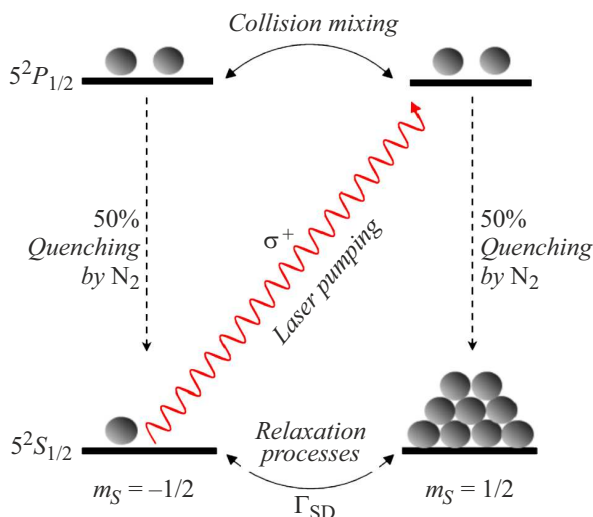


Figure 2. Ballast gas (nitrogen) is needed for non-radiative quenching of excited states of rubidium. The presence of the external field determines the Zeeman levels and allows the pumping of only one transition in accordance with the quantum-mechanical selection rules. This causes atoms accumulation in one of the sublevels, while a reduced number of atoms in another ground state sublevel absorbs the laser light.

Let us assume that atoms placed in a magnetic field have an allowed energy transition that is in resonance with the frequency of the light incident from a light source (it can be a lamp or a laser). Each of the photons has its own angular momentum (spin) equal to 1 (a photon is a boson), and its spin projection on the direction of motion (helicity) has two values only — (± 1). This property in classical electrodynamics corresponds to the circular polarization of an electromagnetic wave [20].

By virtue of the conservation law, when the photon is absorbed by the atom, the total angular momentum does not change, and therefore, after the photon absorption its spin is transferred to the atom. For light with circular polarization, according to the selection rules the transition is possible from the $m_s = -1/2$ sublevel to the $m_s = +1/2$ sublevel (Fig. 2).

Relaxation to the ground state due to collisional mixing of the upper sublevels (N_2 is used as ballast gas) occurs with approximately equal probability both to the lower sublevel $m_s = -1/2$ and to the lower sublevel $m_s = +1/2$. But, since the atom continues to be irradiated, the sublevel $m_s = -1/2$ is gradually emptied, and the sublevel

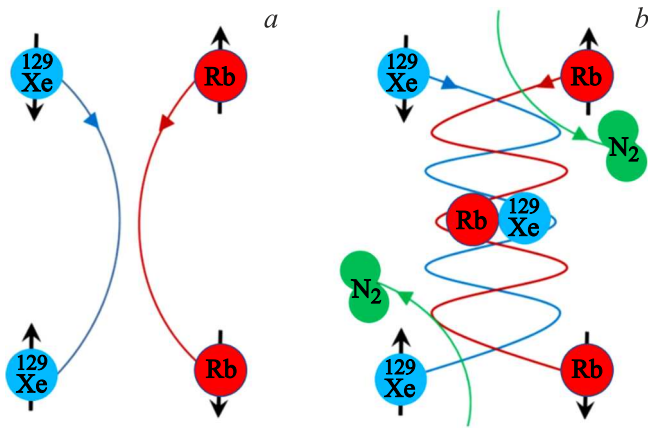


Figure 3. Diagram illustrating the spin exchange between the electron spin of rubidium and the nuclear spin of xenon; *a* — mechanism of binary collisions, *b* — the Van-der-Vaals mechanism of formation and decay of molecules (RbXe). The third body (molecules N_2) (*b*) is required for the simultaneous conservation of energy and pulse.

$m_S = +1/2$ is populated. Theoretically, after some time, determined by the intensity of the incident light and the absorption cross-section of the main transition, all atoms are in the state $m_S = +1/2$ (Fig. 2). For alkali atoms this time actually amounts to several tens of microseconds at a light power of several W. The most suitable for this process was the Rb atom, which has the absorption line with a wavelength of 795 nm [21].

In the second stage of the SEOP process, angular momentum is transferred from the electron spins of the rubidium to the xenon nuclei via collisions in gas phase. These spin-exchange processes can occur in two ways: two-particles collisions (fast process, Fig. 3, *a*) or three-particles collisions with the formation of short-lived dimers due to the nitrogen molecules presence in the gas mixture (Fig. 3, *b*).

In this case, the second mechanism is more efficient under conditions of low density of gases (especially density of Xe) [22]. However, the polarization of rubidium atoms lost as a result of collisions is quickly restored due to photons reabsorption by them, so the spin ordering of Rb atoms lost due to spin-spin interactions is quickly restored if the resonant photon flux is sufficiently high.

To date, the theoretical analysis of the conditions for the spin exchange reactions occurrence between polarized rubidium and ^{129}Xe isotope [10,23–26] was carried out in sufficient details in the scientific literature, and the optimal conditions for obtaining HP xenon-129 [7,27–29] were analyzed. However, there are still some issues that require separate study, but they are not considered in this review.

The development of the method of optical pumping of alkali atoms followed by collisional spin exchange with noble gas isotopes began several decades after the pioneer work of Kastler and colleagues [16] in the studies of Happer et al. [23], which for the first time reported

on the production of hyperpolarized noble gas atoms by the SEOP method. For almost 10 years the process of obtaining the hyperpolarized atoms has been consistently studied, resulting in a gradual transition from obtaining the detectable amount of hyperpolarized gases to the possibility of production and storage of these gases in significant quantities (liters) [7,30,31], which is noted in the reviews [5,32].

In this review, a comparative analysis of the technological developments of installations for the production of HP noble gases is carried out, they are grouped into two classes: „with a stopped-flow“ and „with a continuous flow“. The most significant technical differences between these options of polarizers are in the gas treatment (input to and output from the cells) and in the xenon separation from the gas mixture of the SEOP process. In a stopped-flow device a portion of the required gas mixture is loaded into a SEOP cell containing some amount of alkali metal, heated, and optically pumped by a laser in the presence of an external magnetic field (Fig. 4).

As soon as the magnetic moments of the gas nuclei reach the desired level of polarization, the SEOP process is stopped, and the gas is transferred to a portable storage tank. In the continuous flow device the gas mixture continuously flows from its source through the heated SEOP cell while it is being irradiated with a laser (Fig. 5). The flow rate is chosen in such a way as to provide a sufficient average number of noble gas atoms in the cell, allowing the gas to be polarized „on the fly“. HP xenon can then either be sent to cryogenic storage or directly for medical procedures.

All odd noble gas isotopes can be used in stopped-flow installations, while the relatively high spin exchange rates and light cryopreservation of HP ^{129}Xe make it the best choice for continuous flow devices. Both design options have evolved significantly over the years, reaching an increasing degree of gas polarization and production

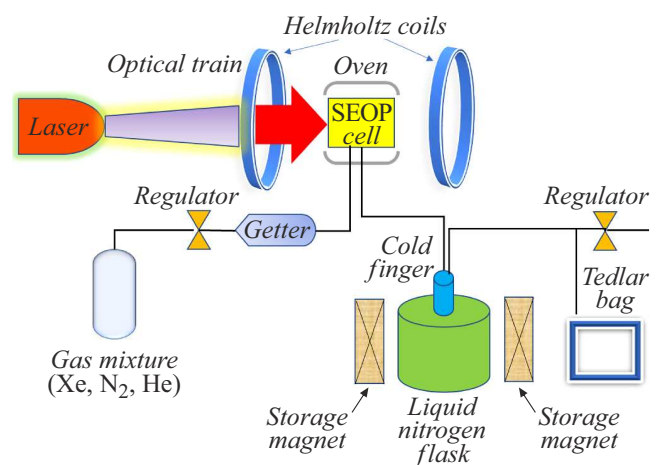


Figure 4. Schematic design when the stopped-flow method is used. The gas mixture is held in the optical cell during the entire SEOP process before being transferred to a container for further use.

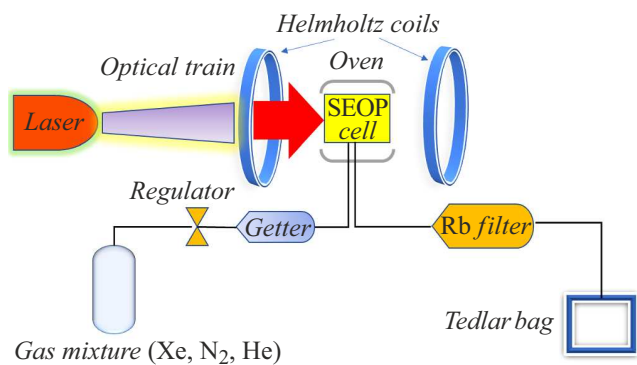


Figure 5. Schematic design when the continuous flow method is used. In the continuous flow polarizer there is a trade-off between gas flow rate and storage time for a given volume of polarized gas.

volumes, in particular, due to the appearance of compact, powerful, relatively inexpensive light sources embodied in spectrally narrowed stack laser diode arrays.

1. Basic elements of polarizer designs

The key parameters affecting the maximum achievable nuclear polarization of ^{129}Xe include the Rb vapor density (directly related to the pumped cell temperature), the pumping gas composition (Xe, N_2 and ^4He), pumping time or flow rate, SEOP cell wall cover, magnetic field strength and uniformity, and laser line spectral width and power [33].

1.1. Lasers

In the early papers, the SEOP method used mainly titanium-sapphire lasers. The output power of these lasers in continuous mode is only a few watts, but the width of the laser emission line is much smaller than the width of the Doppler absorption line of the rubidium atom. As a result, all laser radiation is effectively absorbed by the Rb vapor without any additional devices, and for this reason, the titanium-sapphire laser is well suited for the production of small quantities (about 10 cm^3) of polarized $^{129}\text{Xe} > 50\%$ at a pressure of about 10 to 50 mbar [30,34].

With the appearance of high-power diode lasers operating in the near-IR range, the use of titanium-sapphire lasers has practically ceased. Stack laser diode arrays (LDA) make it possible to obtain output power in the 795 nm line up to 200 W and higher. Such laser arrays are also made in Russia at NPP Inzhekt [35]. With the higher optical power available with LDA, much higher densities of alkali metal atoms can be excited, and the nuclear polarization rate of gas ^{129}Xe is proportionally higher due to the increasing of spin exchange collision rate of Xe–Rb. The higher polarization rate can provide a gas flow such that the Xe/ N_2 /He mixture continuously passes through the cell [36]. Therefore, the use of LDA is preferred in applications

requiring large amounts of polarized gas, such as magnetic resonance imaging [8,27,37].

To reduce the generation line width the diffraction arrays are used both outside the laser cavity and in the intracavity diagram. Fig. 6, *a* shows the optical diagram using a diffraction array outside the laser cavity, and Fig. 6, *b* shows the effect of generation line narrowing at the output of the laser assembly.

With the development of optical technologies, Bragg volume holographic gratings began to be used to narrow and to stabilize the generation lines of high-power diode lasers and laser assemblies. In one of the first papers [39] the narrowing of the generation line of the powerful diode laser by eight times was obtained.

In the paper [40], a volume holographic grating (VHG) was used to narrow the generation line of a high-power diode laser array by almost an order of magnitude (Fig. 7), which made it possible to significantly increase the HP xenon-129 SEOP polarizer efficiency.

Of course, VHG-gratings are more difficult to manufacture and somewhat more expensive than reflective diffraction gratings, but they significantly simplify the optical design and make it easier to set the SEOP polarizers.

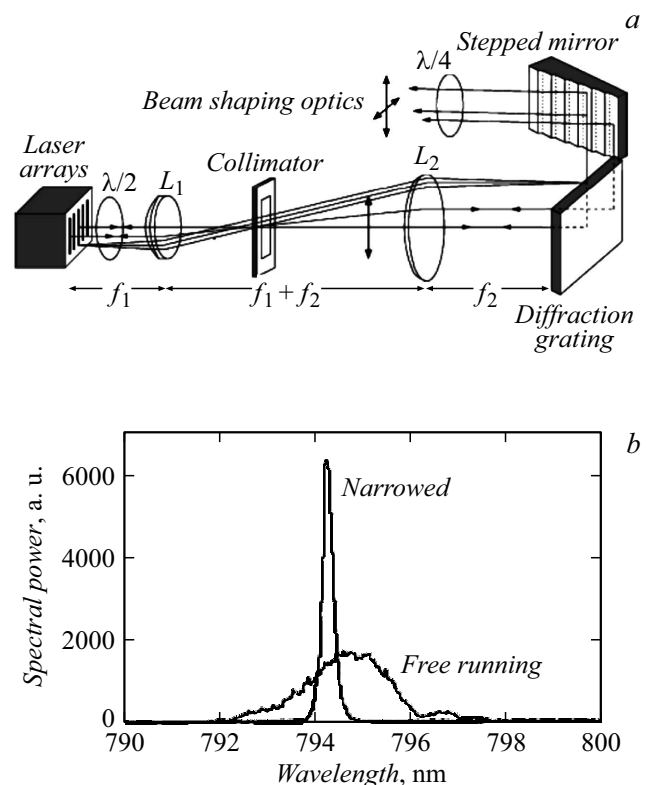


Figure 6. *a* — laser assembly diagram (each of the five diode gratings consists of 49 optically independent emitters) with an extracavity diffraction gratings (1800 grooves/mm): L_1 and L_2 — plane-convex lens and achromatic lens with focal lengths of $f_1 = 250\text{ mm}$ and $f_2 = 500\text{ mm}$ respectively, $\lambda/2$ and $\lambda/4$ — half- and quarter-wave plates; *b* — comparison of free-oscillation linewidth and with the use of extracavity diffraction grating (adapted from [38]).

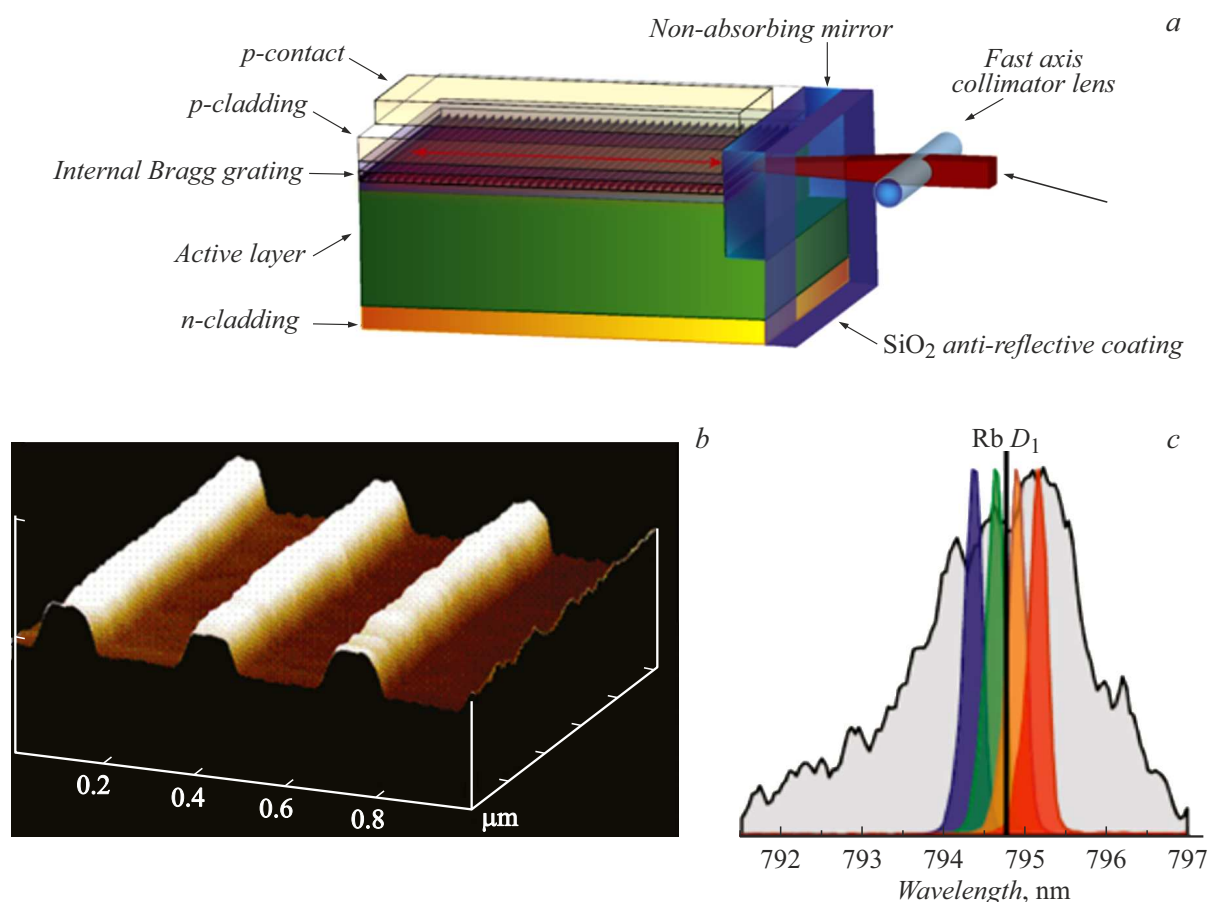


Figure 7. *a* — AlGaAs based LDA diagram, the emission line of which is narrowed in frequency using built-in Bragg gratings, only the path of a single laser beam is shown for simplicity. Bragg gratings were obtained by the method of chemical vapor deposition (MOCVD). After the first epitaxial growth step the gratings are formed by optical lithography into a photoresist layer, followed by an etching step. *b* — AFM image of the internal grating. *c* — typical broadband LDA output spectrum (grey) compared to VHG-LDA examples with frequency narrowing „on chip“ set to different wavelengths (different colors). Adapted from [40].

Narrowing of the generation line of the diode laser assembly does not completely solve the problem of matching the generation line of the laser and the absorption line of rubidium. The half-width of the narrowed generation lines of the diode laser assembly is tens and hundreds of GHz, while the Doppler width of the absorption line does not exceed several GHz [41,42]. One can solve the problem or at least get closer to its solution by increasing the pressure of the working gas mixture (see below).

1.2. Optical diagrams

With the help of linear polarizers and a quarter-wave plate, laser radiation with circular polarization is obtained. This radiation is directed into a cell containing Rb vapor, noble gas (better enriched with ^{129}Xe isotope) and ballast gas, most often nitrogen [21]. Many options of optical diagrams are known, two examples of modern optical diagrams are shown in Figs. 8 and 9.

1.3. Magnetic field

A constant magnetic field in the range of 10 to 100 mT is created by Helmholtz coils (Fig. 10), which allows access to the SEOP cell, or solenoids (Fig. 11).

The functions of this element of polarizers design are as follows:

- Ensuring effective spin polarization of rubidium atoms in the process of optical pumping of its energy levels;
- Maintaining the polarization of nuclear spins of ^{129}Xe ;
- Creation of conditions for NMR diagnostics of the degree of their polarization.

Experimental monitoring of spin polarization carried out in paper [31] is illustrated in Fig. 12.

When B_0 is „off“ (left), optical pumping, i.e. the creation of a thermodynamically nonequilibrium configuration of the magnetic moments of rubidium valence electrons is inefficient, which leads to almost equal populations of their ground spin states ($m_s = +1/2$ and $-1/2$) and a high density of absorption centers in the gas phase (Fig. 12, inset on the left). The magnetic field application along

the quantization axis, whose orientation is set by the laser with polarized radiation, leads to efficient optical pumping and uneven population of the ground state of rubidium atoms: accumulation of electrons in the state with $m_S = +1/2$ and the decreasing number of atoms in the state with $m_S = -1/2$. In the first case, the electrons do not change their state during irradiation, and their number increases due to the electrons of the atoms returning from the excited state to the ground state, which corresponds to a high electron spin polarization and leads to the laser transmission increasing (Fig. 12, inset on the right).

The example of the magnetic field B_0 effect on the polarization of ^{129}Xe nuclear spins is shown in Fig. 13.

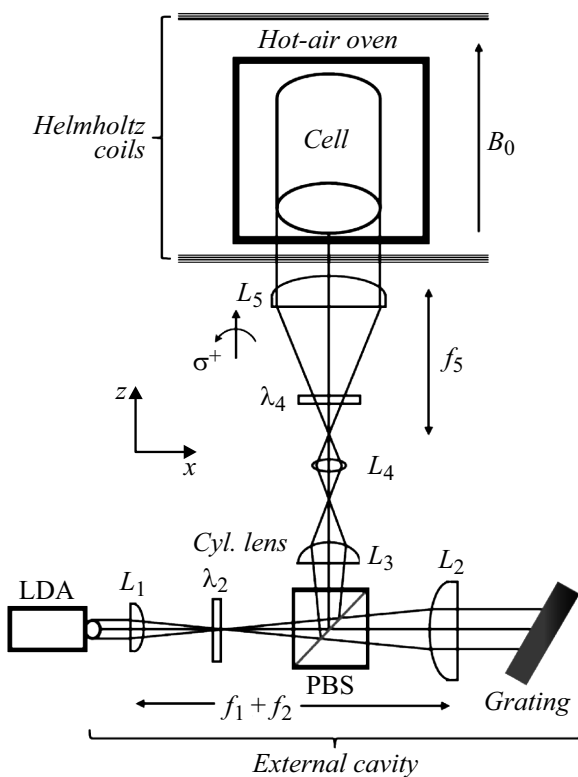


Figure 8. Optical diagram of laser unit with beam formation and polarization optics: LDA — laser diode array; L_1 – L_3 — cylindrical lenses with focal lengths of $f_1 = 62$, $f_2 = 250$ and $f_3 = 80$ mm; L_4 — biconvex lens with focal length of $f_4 = 80$ mm, L_5 — plane-convex lens with focal length of $f_5 = 250$ mm, PBS — cubic polarizing beam splitter, $\lambda/2$ and $\lambda/4$ — half- and quarter-wave plates (adapted from [43]).

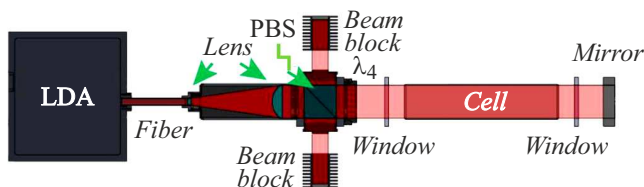


Figure 9. Optical diagram of laser unit used in XeUS polarizers (adapted from [44]).

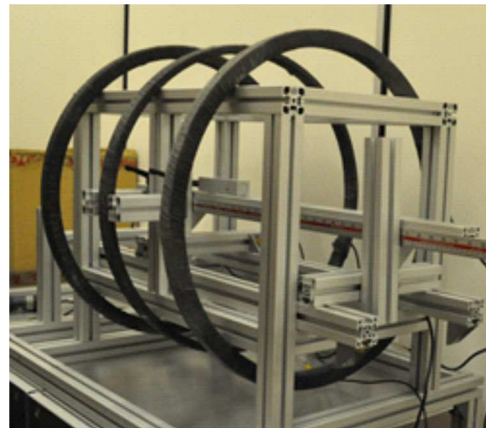


Figure 10. Three-component Helmholtz coils during polarizer mounting (adapted from paper [44]).

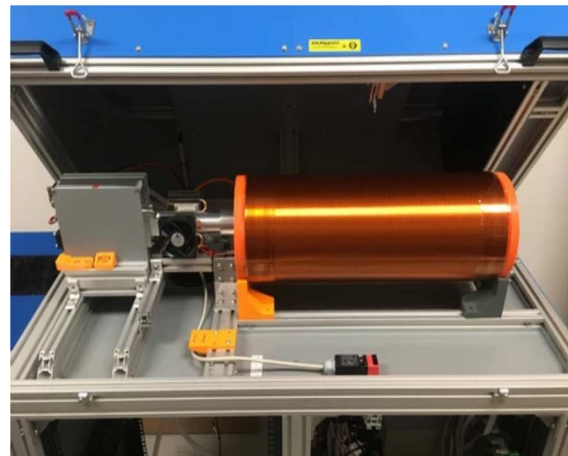


Figure 11. Electromagnet with SEOP cell placed inside it [45].

1.4. Composition of gas mixture

Attempts are made to increase the width of the rubidium absorption line, first of all, by increasing the gas mixture pressure (Fig. 14). It is helium in the gas mixture that serves as the main buffer gas to achieve this goal.

1.5. SEOP cell

Inside such cells the SEOP process is implemented, and therefore they are usually made of Pyrex glass, which is a borosilicate glass of composition: SiO_2 at least 80%, (12–13)% B_2O_3 , (3–4)% Na_2O and (1–2)% Al_2O_3 (Fig. 15).

The softening temperature of this type of glass to dynamic viscosity is (580–590)°C. It is suitable for operation at temperatures up to 800°C at atmospheric pressure and maximum 650°C when operating in vacuum. Unlike quartz glass Pyrex glass up to 650°C is practically impenetrable for N_2 , O_2 , H_2 , He. Based on the combination of properties,

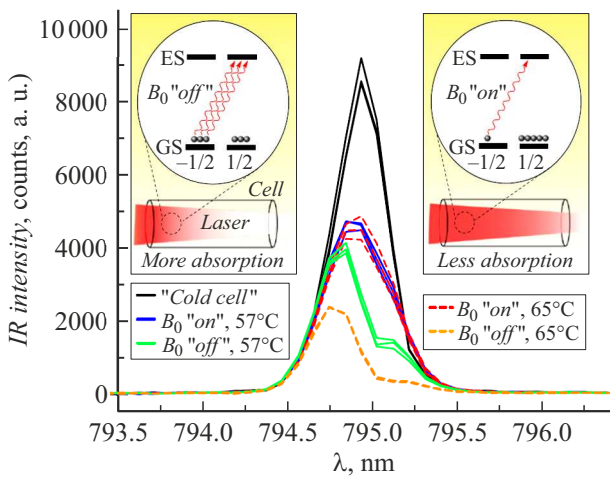


Figure 12. Monitoring of spin polarization of Rb electrons during SEOP. Lines of laser IR radiation transmitted through the SEOP cell are shown. Black lines are „cold cell“ at two temperatures; blue lines (in the online version) — $T = 57^\circ\text{C}$ and $B_0 = 5.26\text{ mT}$; green lines (in the online version) — $T = 57^\circ\text{C}$ and $B_0 = 0\text{ mT}$; red dashes (in the online version) — $T = 65^\circ\text{C}$ and $B_0 = 5.26\text{ mT}$; orange dashes (in the online version) — $T = 65^\circ\text{C}$ and $B_0 = 0\text{ mT}$. The insets show the effect of depleting Rb vapor pumping on the intensity of radiation transmitted by the laser with circular polarization σ^+ (ES and GS are excited and ground states, respectively). Adapted from paper [31].

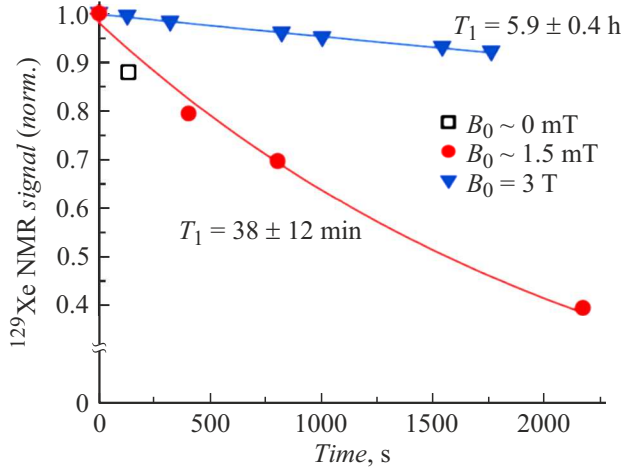


Figure 13. Spin-lattice relaxation time (T_1) of NMR signals from HP ^{129}Xe . Xe gas is transferred to Tedlar sampling bags at 3 T during the entire decay (blue triangles (in the online version)) or stored at $\sim 1.5\text{ mT}$ (red circles (in the online version)) or $\sim 0\text{ T}$ (white square) and quickly transferred to 3 T field for NMR measurements. Adapted from paper [31].

borosilicate glass is preferable to quartz for use in SEOP optical cells.

The loss of hyperpolarization on the cell walls can be greatly accelerated in the presence of even a small amount of ferromagnetic material. The presence of iron and nickel in glass, even at levels of a few ppm, can adversely affect

process capacity and ^{129}Xe storage capacity [47]. For this reason, the internal surfaces of SEOP cell of glass gas paths are coated with various organic polymeric materials. One of such material is siloxane [48].

1.6. Oven

The polarizer oven is one of the key subsystems. Its role is to maintain and thermally control the optical cell during the experiment, as well as to increase and to decrease the operating temperature of the cell at the beginning and end of SEOP experiments. In modern polarizers the oven is heated and cooled by a thermoelectric cooler (TEC). This method eliminates the need for liquid nitrogen or heat exchange fluids for a forced-air oven. The heating power is

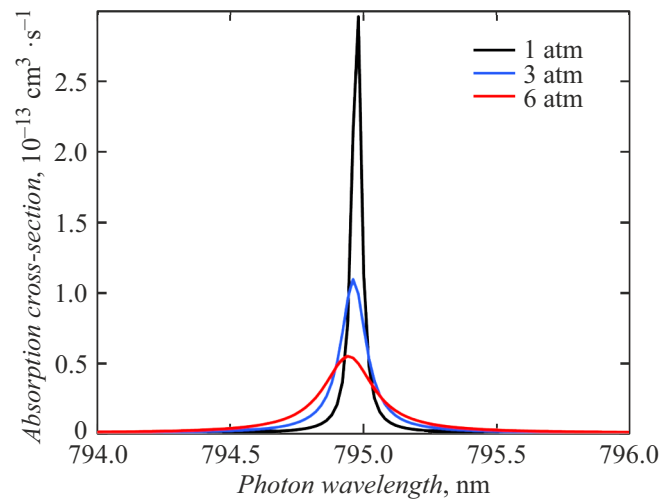


Figure 14. Rb-D1 absorption cross-section of gas mixture consisting of 1% Xe (a natural mixture of isotopes), 10% N_2 and 89% He (by volume) at several operating pressures (adapted from paper [46]).

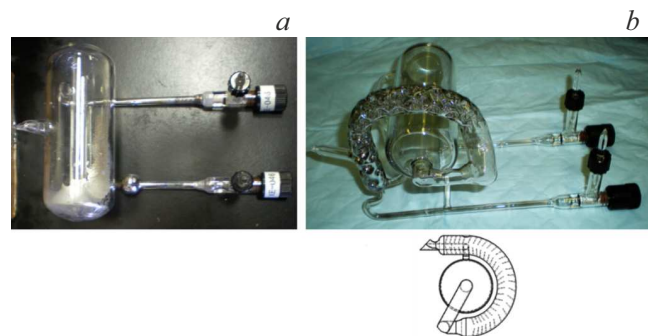


Figure 15. Design of polarizer optical cell. Two generations of SEOP cells. *a* — the initial design, in which a tiny spherical Rb presaturation bulb is visible on the inlet rod, but the major portion of Rb is housed in the cell body; *b* — Vigreux design with significantly increased presaturation area. As compared to the standard cell that operates at temperatures of $150\text{--}170^\circ\text{C}$, Vigreux cells operate at $110\text{--}120^\circ\text{C}$ and Rb presaturation area is heated to $\sim 190^\circ\text{C}$. Adapted from paper [46].

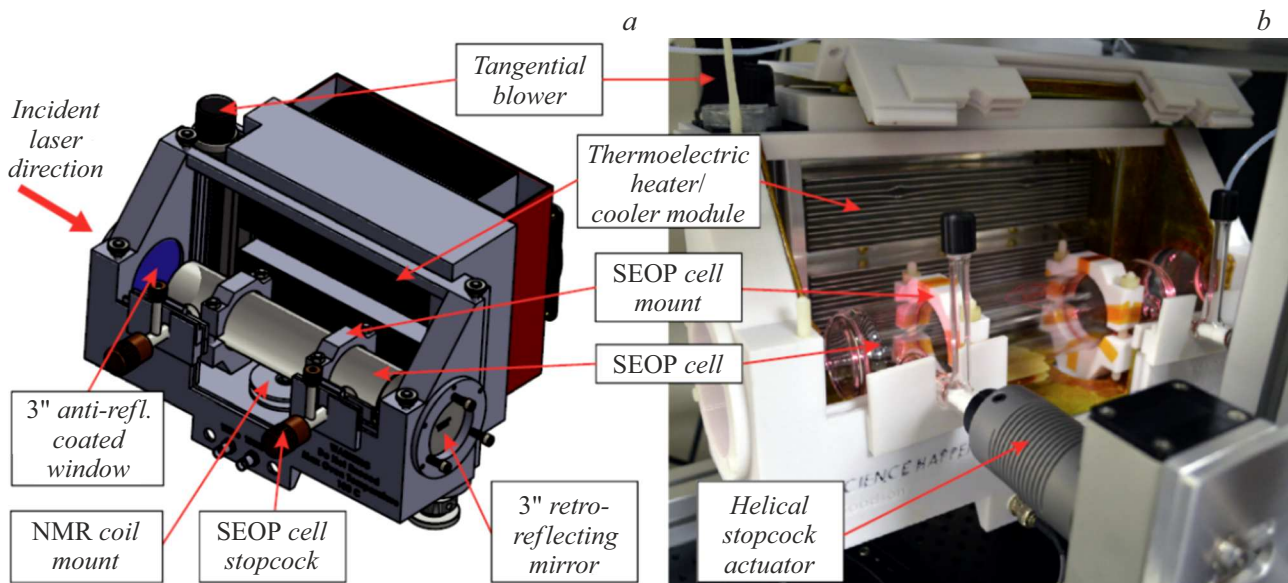


Figure 16. *a* — 3D-model showing the SEOP cell and forced-air oven; *b* — photo of the actual unit. Adapted from paper [45].

distributed inside the oven by a fan located in the corner of the oven. The rotary fan circulates the air inside the oven moving actively heated (or cooled) air from the immediate vicinity of the TEC to the optical cell and back. An option of the oven design obtained by the 3D-printing method is shown in Fig. 16.

An important thermal control factor is related to the fact that during the interaction of laser radiation with the contents of the optical cell a significant part of the laser power is dissipated in the cell leading to additional heating. For this reason, the input thermal heating power must be reduced in a controlled manner during operation from its initial level.

1.7. Gas manifold

The purpose of this structural element of the polarizer is to prepare the necessary composition of the gas mixture for the SEOP process implementation. There are a huge number of implementation options, but the main structural parts of the gas manifold are well represented in Fig. 17.

1.8. NMR detection of xenon polarization

The resonant frequency of NMR of xenon nucleus is proportional to the magnetic field in accordance with the fundamental Larmor relation

$$f = \frac{\gamma}{2\pi} B \quad \text{or} \quad \omega = \gamma B,$$

where γ is the gyromagnetic ratio. For ^{129}Xe nuclei $\gamma/2\pi = 11.777 \text{ MHz/T}$, while for ^1H nuclei $\gamma/2\pi = 42.576 \text{ MHz/T}$ [3]. Usually this frequency is chosen in such a way that it falls into the band with the least amount of external noise. Low current in B_0 coils is desirable to

minimize resistive heating from B_0 coils, but a higher field is required to increase the water signal polarization when calibrating the polarizer. Consider that whatever frequency is chosen for the water signal calibration, the power supply for B_0 coils must be able to achieve four-fold current to drive the xenon NMR resonance to the same calibration frequency.

When using low fields B_0 , the Larmor frequency is reduced to the values of several tens of kHz, and this not only simplifies the requirements for electronics, but also provides a significant advantage for MRI in the volume of tissues, since radiation with such frequency passes through the skin and electrically conductive areas of tissue more easily [21].

1.9. Storage and transportation

To preserve the nuclear polarization of frozen xenon during storage and accumulation, it is necessary to maintain it in a sufficiently strong magnetic field, about hundreds of mT [50]. In papers [51,52] the relaxation properties of Xe ice are characterized in detail at various magnetic fields and temperatures. At 77 K the relaxation time constant (T_1) is 2.5 h for a field stronger than 0.07 T. If solid ^{129}Xe is heated above 77 K, then its T_1 becomes shorter. Moreover, at temperatures above 120 K ^{129}Xe T_1 becomes more dependent on the strength of the magnetic field, and increasingly higher fields are required for its long-term storage. For 160 K and field 0.2 T the time T_1 is reduced to ~ 2 min [51,53].

One of the promising options of the cryostorage system, which significantly (up to 50%) reduces the polarization losses of ^{129}Xe , is shown in Fig. 18.

Currently, constant magnetic fields in the range from 0.05 to 0.3 T are created by Halbach magnets (Fig. 19).

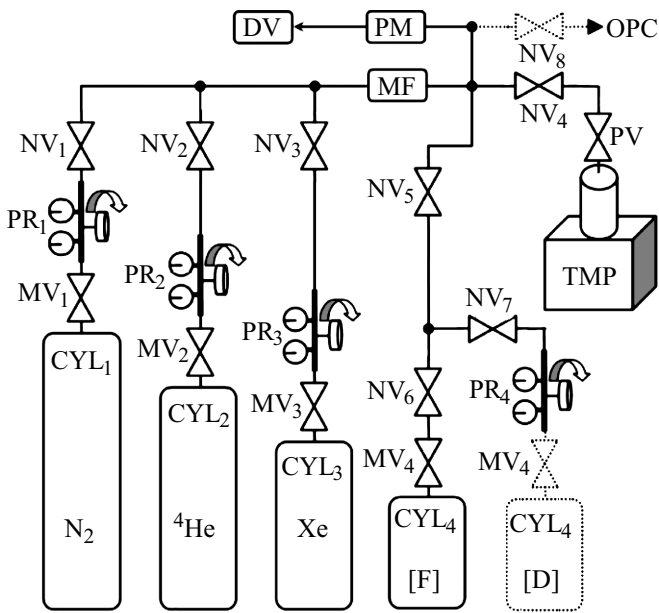


Figure 17. Gas manifold diagram: CYL1–4 — gas cylinders, MV1–4 — main valves, MV1–4 — precision reducers, NV1–8 — needle valves, MF — microfilter, PM — precision pressure meter, DV — digital voltmeter, PV — pump valve, TMP — turbomolecular pump; OPC — gas line connector to SEOP cell (adapted from paper [49]).

The Halbach matrix is a special and interesting system of permanent magnets developed at Lawrence Berkeley National Laboratory in 1979. The matrix was originally invented by K. Halbach to help particle accelerators in beams focusing. The direction of magnetization of each two adjacent magnets in the Halbach lattices differs by a certain angle, then the magnetic field creates an asymmetric distribution.

The Halbach magnet with a cold pin inside is placed in the Dewar flask filled with liquid nitrogen. The Dewar flask can be transported to its final destination where the polarized xenon can be thawed. The loss of polarization during the whole procedure, including the 30 minute transport time, is about 50% of the initial level [49].

2. Analysis of polarizer designs

2.1. Historical note

In the first part of the analytical review, we will provide only summary information on the developments of period 1999–2010, which will give the reader an idea of the history of the development of this technical direction.

2.1.1. Lasers

The optical pumping of rubidium atoms was carried out using broadband (2–3 nm) diode lasers arrays (LDA) of medium power (from 25 to 60 W [54–62]) and high power (from 100 to 210 W [30,36,63–70]). And only at the

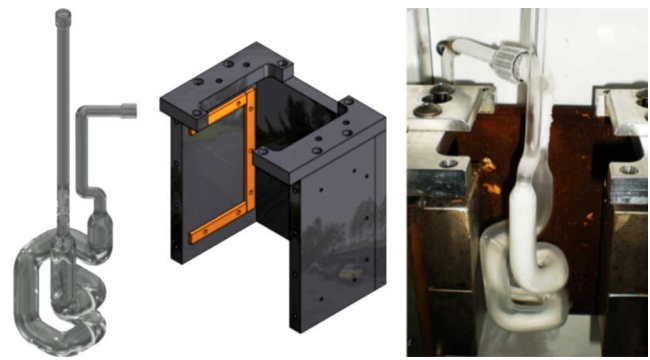


Figure 18. A cold trap like „puzzle“ (left), filled with a portion of frozen xenon inside a magnetic yoke (right). There is very little xenon at the exit of the cold pin, indicating complete extraction. The model of the magnetic yoke is shown in the center of the Figure, and on the right its implementation is shown. High-strength permanent magnets are attached to the brackets shown in orange. The sides of the yoke are made of material with high magnetic permeability, and the top brackets are made of aluminum. The front panel of the yoke is not shown. The field on the yoke axis is 0.2 T. Adapted from paper [46].

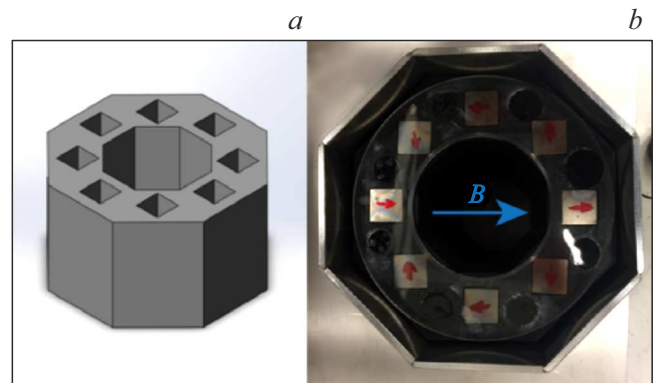


Figure 19. Halbach magnet example: *a* — model, *b* — 3D printed Halbach matrix with neodymium magnets. The arrow indicates the direction of the magnetic field. Adapted from paper [49].

end of the first decade of the XXI century the medium-power LDAs with 3D holographic Bragg gratings began to be actively used, which made it possible to sharply (to 0.1–0.3 nm) narrow the width of the radiation line of the pumping laser, thus significantly increasing the efficiency of the laser power use in the SEOP process [71–73].

2.1.2. Gas mixtures

Their composition varied near the relation 96–98% ⁴He, 1–2% N₂ and 1–2% Xe of natural content (26.4% ¹²⁹Xe) or enriched by ¹²⁹Xe (81 to 93% [59,60,61,63,67]). Two groups of units were determined clearly by the mixture pressure in the SEOP cell: the first group — low pressures (from 0.05 to 2 bar [54,58,59,62,65,69,71,73]) and the second group — high pressures (from 3 to 8 bar [30,36,55,56,57,60,63,64,68,70,72]).

2.1.3. SEOP cells

Most polarizers used cells from 100 to 300 cm³, and only a few designs were with cells larger than 1000 cm³ ([71,73]).

2.1.4. Magnetic field

Basically, the developments mentioned above used Helmholtz coils or multilayer solenoids with fields from 1 to 6 mT to implement the SEOP process. However, versions of polarizers without such additional design parts were demonstrated: for the SEOP process they use a scattered field (10–40 mT [54,61,65–68]) from a powerful superconducting magnet used for NMR tomography (as a rule, these are magnets with fields from 1.5 to 11 T).

2.2. Modern designs of xenon polarizers

2.2.1. Stopped-flow polarizers

2.2.1.1. Kraków

The paper [49] describes the design of the optical pumping polarizer with spin exchange for ¹²⁹Xe operating in the stopped-flow mode. In such polarizer it is possible to obtain in one cycle 30–60 cm³ of polarized xenon-129 during 10–15 min using a low-power laser (9 W) and SEOP cells of about 1000 cm³. The polarization of xenon-129 nuclei reaches about 40% in a gas mixture containing 3% of isotopically -enriched xenon (up to 91% relating ¹²⁹Xe). Hyperpolarized xenon is accumulated in a removable Dewar vessel with liquid nitrogen containing the Halbach magnet with a field of 600 mT and cold trap inside.

2.2.1.2. Nottingham

Researchers from the University of Nottingham (United Kingdom) proposed and studied [74] the concept of the stopped-flow SEOP with concentrated noble gas mixtures at low pressures. For ¹²⁹Xe SEOP without cryogenic separation the highest obtained intensity of the NMR signal from the gas mixture of HP xenon and nitrogen was equivalent to the intensity occurring at 15.56–1.9% of spin-polarized ¹²⁹Xe in pure gaseous xenon. The productivity of the HP gas mixture, measured at 298 K, was 1.8 cm³/min. This paper demonstrated that the SEOP process with mixtures containing high concentrations of xenon (5 to 72%) can produce high spin polarization (65 to 15%, respectively) at 100°C and pressure of 100 kPa (0.1 bar). This concept can be used as a route to MRI using HP noble gas without the need for cryogenic separation, which requires compression of HP xenon after the process of the NMR scanner operation. As shown earlier [61], the membrane pumps can be used to compress low pressure ¹²⁹Xe after SEOP without significant depolarization. It was shown in paper [74] that recompression maintains about 80% of the ¹²⁹Xe polarization.

2.2.1.3. XeUS GEN-1

The paper [75] shows that the use of the 3D-printing method greatly simplifies the integration of key components with the variable temperature of the SEOP cell:

- (i) NMR circuit *in situ* operating at a frequency of 84 kHz (the Larmor frequencies of nuclear spins ¹²⁹Xe and ¹H),
- (ii) laser emitter 200 W with a half-width below 0.3 nm,
- (iii) *in situ* high resolution spectroscopy of close IR range,
- (iv) thermoelectric temperature monitoring,
- (v) reflective optics.

The SEOP unit is described for obtaining values of ¹²⁹Xe polarization approx 74 ± 7% in a cell 0.51 at a xenon partial pressure of 1000 Torr. High values are obtained for the exponential rate of ¹²⁹Xe polarization rise (0.63 · 10⁻³ s⁻¹) and the time of spin-lattice relaxation in cell (T₁ = 2.19 h) for 1000 Torr Xe.

2.2.1.4. XeUS GEN-2

The papers [45,76] describe the ¹²⁹Xe polarizer intended for the production of HP xenon with the capacity sufficient for medical researches without use of HP xenon cryostorage system. The partial pressure in the SEOP cell is from 0.66 to 2.5 bar. The 3D-printed polycarbonate oven equipped with thermoelectric cooler/heater ensures the thermal stability of the SEOP cell when using both binary blends (Xe/N₂) and ternary blends containing also helium. The degree of xenon polarization (P_{Xe}) 93.2 ± 2.9% in the cell is achieved at the xenon partial pressure of 0.66 bar and the polarization rise rate γ_{SEOP} = 0.040 min⁻¹, which is equivalent to the capacity of 0.11 l/h on 100% HP and 100% enriched ¹²⁹Xe. The xenon partial pressure increasing to 1.75 bar leads to the capacity rise to 0.3 l/h, but P_{Xe} drops to 72.6 ± 1.4%.

2.2.1.5. XeUS GEN-3

The paper [77] describes a third generation automated xenon-129 polarizer (GEN-3) using a continuous high power (~ 170 W) of laser radiation and a new design of the aluminum shell to quickly increase the temperature of gas mixtures rich in xenon (partial pressure up to 2 bar). The aluminum shell design is capable of heating the SEOP cell from ambient temperature (typically 25°C) to 70°C (SEOP process temperature) in 4 min, and cooling the cell to the temperature at which the HP gas mixture can be released from the cell in about 4 min. Levels of xenon hyperpolarization exceeding 40% were reached at the rate of xenon spin order rise γ ≈ 0.1 min⁻¹. A record-high time of longitudinal relaxation of xenon nuclear spins (T₁) in the SEOP cell, exceeding 2.5 h at room temperature, was obtained. A step-by-step scheme of the operation of this polarizer is shown in Fig. 20 along with graphs illustrating the individual stages of its operation.

2.2.1.6. TR-SEOP

The paper [78] describes the process of optical pumping with spin-exchange with temperature increasing (TR-SEOP) in the automated stopped-flow hyperpolarizer using three key temperature modes:

- (i) „hot“ when ¹²⁹Xe hyperpolarization is at its maximum,
- (ii) „warm“ when ¹²⁹Xe hyperpolarization approaches 1, and
- (iii) „cold“ when HP ¹²⁹Xe gas is transferred to the Tedlar bag for storage.

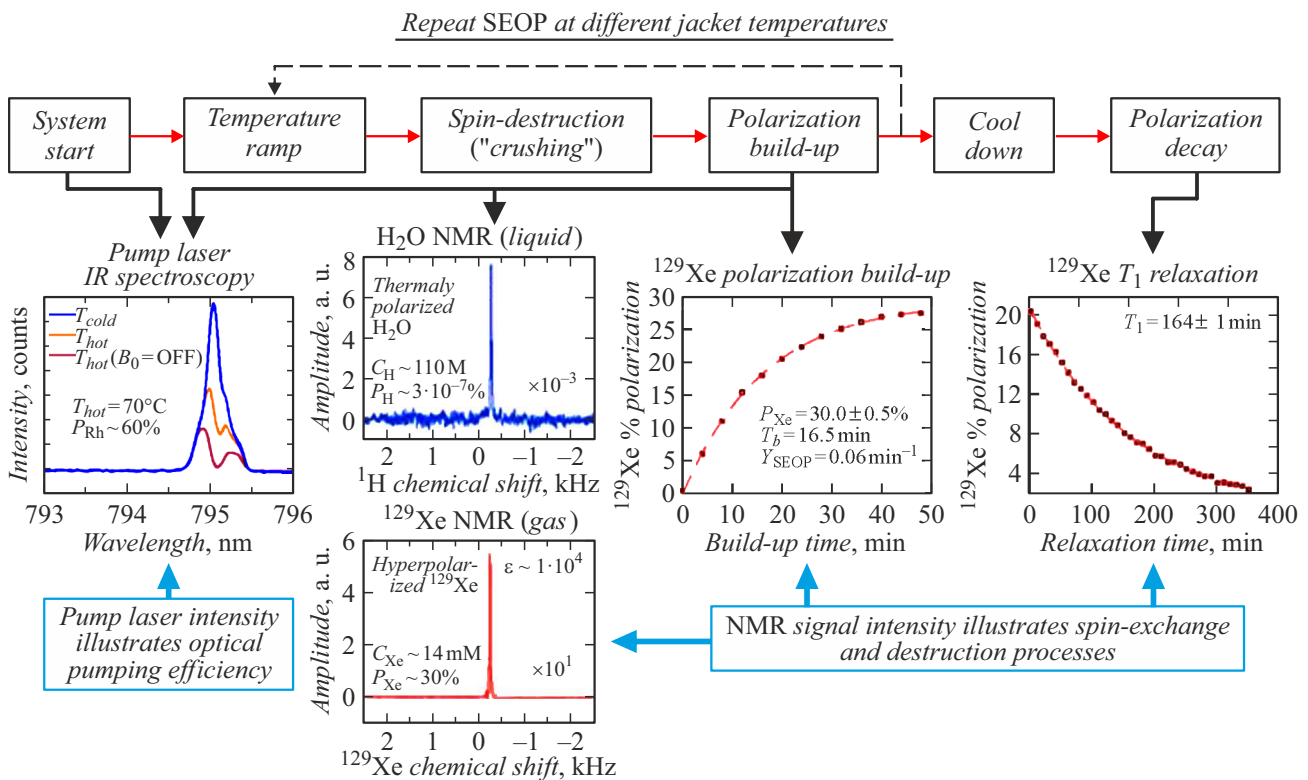


Figure 20. Block-diagram describing typical operation stages of the hyperpolarized device GEN-3. Example of data: *a* — absorption spectra of laser radiation used to estimate the electron polarization of Rb (PRb); *b* — NMR spectroscopy on ^1H thermally polarized water phantom nuclei; *c* — NMR spectroscopy on ^{129}Xe used to measure the nuclear spin polarization (P_{Xe}) relative to the proton phantom polarization; *d* — ^{129}Xe polarization rise curve used to calculate the rise rate of ^{129}Xe (γ_{SEOP}) and stable P_{Xe} ; *e* — polarization relaxation curve of ^{129}Xe used to calculate ^{129}Xe (T_1) decay rate. Adapted from paper [77].

Unlike the traditional approach of SEOP in batch mode, here all three temperature modes can work in continuous flow mode. The variable temperature approach increased the SEOP rate by more than two times as compared to the rate of polarization at constant temperature (e.g. providing effective values for the exponential rise constant γ_{SEOP} ($62.5 \pm 3.7 \cdot 10^{-3} \text{ min}^{-1}$ vs. ($29.9 \pm 1.2 \cdot 10^{-3} \text{ min}^{-1}$) when reaching almost the same maximum value P_{Xe} ($88.0 \pm 0.8\%$ vs. ($90.1 \pm 0.8\%$) at the load of Xe cell 500 Torr (67 kPa). The contrast increasing was shown of images of magnetic resonance imaging in fields 3 T and 4 mT by $\sim 3.1 \cdot 10^5$ and $\sim 2.32 \cdot 10^8$ times, respectively.

2.2.1.7. XeNA

The paper [31] presents the design of the ^{129}Xe polarizer with a capacity of about 1l/h, proposed for preclinical, clinical and MRI studies. The device uses a powerful laser diodes array (up to 200 W in the Rb D1 line) and a gas mixture with high xenon content (up to 1800 Torr Xe in 500 cm³). The degrees of xenon polarization (P_{Xe}) in the cell ~ 90 , ~ 57 , ~ 50 , and $\sim 30\%$ were obtained using gas mixtures with xenon partial pressures of 300, 500, 760 and 1570 Torr, respectively. After pumping HP xenon into Tedlar bags and transporting to a clinical 3 T scanner for MRI imaging, the values $P_{\text{Xe}} \approx 41$ and $\approx 28\%$

were obtained (for partial pressures of Xe 760 Torr and 1545 Torr respectively). The degree of spin polarization of ^{129}Xe nuclei was measured by three independent methods, which gave well consistent results:

- (a) NMR sensor on SEOP cell in the field of 52.6 mT, calibrated by the NMR signal from ^1H nuclei,
- (b) gas transportation to NMR spectrometer with the field of 47.5 mT, calibrated by the NMR signal from ^{13}C nuclei;
- (c) gas transportation into MRI tomograph with the field of 3 T. We also measured the polarization decay times ^{129}Xe in a portable storage (Tedlar bag) at room temperature ($T_1 \approx 38$ min and ≈ 5.9 h in magnetic fields of 1.5 mT and 3 T, respectively, which is quite sufficient for various applications of HP xenon.

Detailed information on modern xenon polarizers with „stopped-flow“ are presented in Table 2.

The SEOP process in modern stopped-flow units was modeled in paper [81] in order to study ways to increase the efficiency of HP Xe production in the ^{129}Xe polarizer at high laser fluxes. It is shown that the use of narrower laser lines at a high content of xenon in the mixture should lead to HP ^{129}Xe production increasing. Calculations showed that a 3” SEOP cell should double the magnetization yield as compared to the 2” cell currently used in practice, but

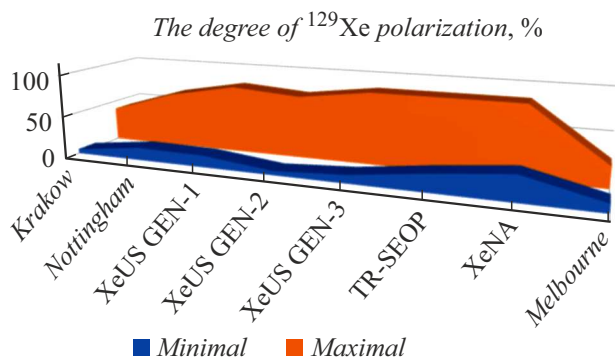


Figure 21. Minimum and maximum degree of polarization of ^{129}Xe nuclear spins at different units.

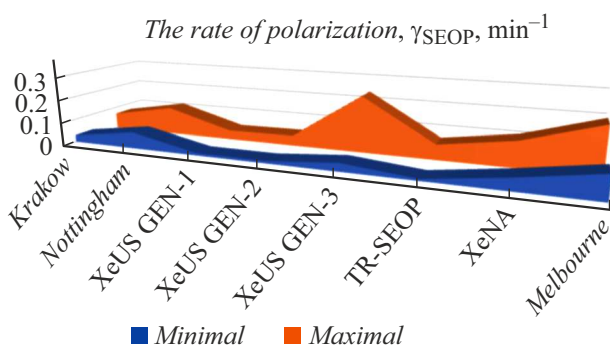


Figure 22. Polarization setting rates in stopped-flow units.

this would require modification of the polarizer components such as the optical circuit, windows with anti-reflective coating, reflectors, and oven.

2.2.1.8. Comparison of „stopped-flow“ polarizers

It can be seen from the data given in Table 2 that all units are designed for the production of gas mixture containing nuclei of polarized ^{129}Xe at pressures ranging from 0.1 to 3 bar and temperatures of 70 to 140°C. Variations in the degree of polarization are shown in Fig. 21. Fig. 22 shows a diagram in which „stopped-flow“ units are compared by such an important parameter as the rate of establishment of spin ordering (polarization rise).

2.2.2. Continuous Flow Polarizers

2.2.2.1. Osaka

The paper [82] presents a new method for the continuous production of concentrated HP gas xenon-129 from gas mixture of diluted xenon (Xe) with high nuclear spin polarization during isobutene SEOP as an alternative to nitrogen (N_2) in the low pressure SEOP unit described in paper [61]. In contrast to the commonly used extraction method by Xe freezing, after the SEOP process isobutene was separated as a liquid at a moderately low temperature (203 K, liquid methane), so that HP Xe was constantly maintained in a gaseous state. This provided a continuous supply of highly polarized concentrated Xe gas to the NMR spectrometer and tomograph.

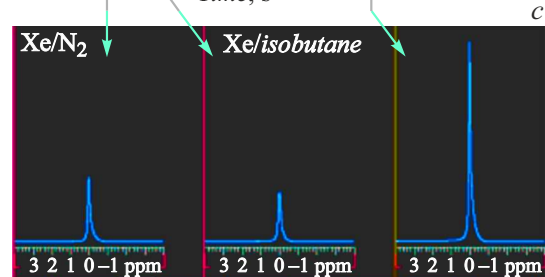
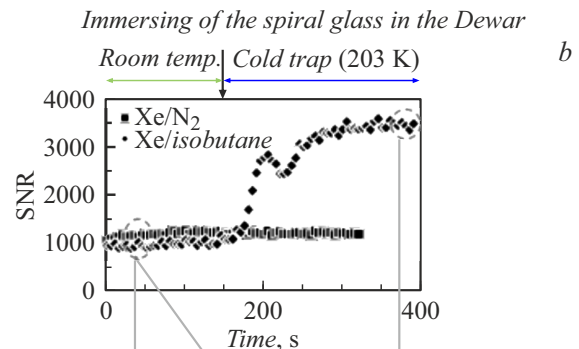
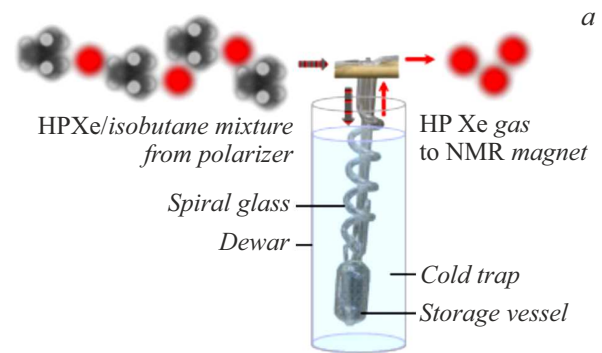


Figure 23. Dynamics of ^{129}Xe NMR signal amplification upon isobutene removal. *a* — diagram of device for the condensation and storage of isobutene using a cold trap; *b* — ratio „signal–noise“ of NMR spectrum ^{129}Xe using Xe/isobutene (diamonds) and Xe/ N_2 (rectangles) gas mixtures vs. time. The spiral glass tubing was immersed in the Dewar flask for isobutene trapping at 203 K at the time indicated by the black arrow; *c* — NMR spectrum of HP ^{129}Xe obtained for Xe/ N_2 gas mixture (left) and Xe-isobutene gas mixture recorded before (center) and after isobutene separation using the cold trap (right) [82].

At the present time, the only effective way to concentrate HP ^{129}Xe for these purposes is buffer gases separation during freezing followed by thawing. The „freezing–thawing“ approach, however, has some disadvantages, such as the time it takes to accumulate enough HP ^{129}Xe solids (takes, for example, several tens of minutes). Although the longitudinal relaxation time T_1 of solid ^{129}Xe at a temperature of liquid N_2 in the presence of a magnetic field is large enough to accumulate [51], this often leads to an additional significant loss of the degree of polarization of ^{129}Xe during its solidification, accumulation, and evaporation. A significant (up to four times) improvement of the NMR signal amplitude on ^{129}Xe nuclei was shown with a simultaneous increase in the ratio „signal–noise“ of

Table 2. Free data on the designs of stopped-flow polarizers for period 2011–2021

Design	LDA power (W), and width line (nm)	Polarization xenon, %	Composition of gas mixtures, partial pressure	Cell dimensions SEOP, temperature process	Magnetic SEOP field, mT	Frequency NMR	Rate of rise polarization $\rho_{SEOP}, \text{min}^{-1}$	Reference
Kraków	9 0.9	5–40	^{129}Xe (91% enrichment) of 3 to 6%. Standard mixture: ratio of components in mixture $^{129}\text{Xe} : ^4\text{He} : \text{N}_2$ is equal to 3.2 : 71.7 : 25.1. Mixture pressure 1.25 bar	Inner diameter 5.6 cm, length 41 cm. Volume 1010 cm ³ 110–140°C	3.65	36.3 kHz	0.03–0.07	[69]
Nottingham	23.3 0.35	15–65	Xe natural composition: (5%, 24.3%, 40.3%, 50%, 72.3%) in mixture with N ₂ and He. Standard mixture 5% Xe, 5% N ₂ , 90% ⁴ He at 2.3 bar	Internal diameter 2.8 cm, length 12.0 cm. Volume 75 cm ³ 100°C	50 Magnet leakage field 9.4 T	External spectrometer 110.6 MHz, 9.4 T	0.07–0.12	[74]
XeUS GEN-1	150–200 0.3	14–80	Xe natural composition at 0.27 or 1.33 bar, N ₂ — up to 2.67 bar	Internal diameter 5.4 cm, length 24.8 cm Volume 500 cm ³ 62–85°C	7.13	84 kHz External spectrometer 558.6 kHz 47.5 mT	0.01–0.04	[75]
XeUS GEN-2	170 0.3	5–74	Xe natural of composition (pressure in bar): 1.33 Xe/1.2 He/1.33 N ₂ 1.77 Xe/1.6 He/130 N ₂ 1.33 Xe/1.33 N ₂ 1.77 Xe/1.77 N ₂	Internal diameter 5.4 cm, length 24.8 cm Volume 500 cm ³ 55–70°C	4.1	40.8 kHz	0.01–0.044	[45]
XeUS GEN-3	170 0.15	10–85	Xe natural of composition (pressure in bar): 1.33 Xe /1.2 N ₂ /0.133 ⁴ He 2.0 Xe/0.66 N ₂	Internal diameter 5.4 cm, length 24.8 cm Volume 500 cm ³ 45–80°C	3.5	40.8 kHz	0.035–0.24	[77]
TR-SEOP	170 0.3	21–85	Xe natural of composition (pressure in bar): 0.66 Xe/2.0 N ₂	Internal diameter 54 mm, length 248 mm Volume 500 cm ³ 45–80°C	4.0	47 kHz	0.008–0.065	[78]

Table 2 (continued).

Design	LDA power (W), and width line (nm)	Polarization xenon, %	Composition of gas mixtures, partial pressure	Cell dimensions SEOP, temperature process	Magnetic SEOP field, mT	Frequency NMR	Rate of rise polarization $\gamma_{SEOP}, \text{min}^{-1}$	Reference
XeNA	200 0.27	30–85	Xe natural composition or enriched (86%) at 0.4–1.7 bar, rest — N ₂ up to 2 bar	Internal diameter 54 mm, length 248 mm Volume 500 cm ³	5.26	62 kHz External spectrometer 559 kHz 47.5 mT External 34.09 MHz 3 T	0.05–0.11	[31,76]
Melbourne	4 × 60 0.3	25	¹²⁹ Xe (86% enrichment) — 0.5 bar, N ₂ — 1.5 bar	Internal diameter 12 cm, length 8 cm. Volume 900 cm ³ 80–120°C	1.0	11.82 kHz External spectrometer 34.09 MHz 3 T	0.1–0.2	[80]

this signal, which opens up the possibility of increasing the NMR tomography sensitivity (Fig. 23).

2.2.2.2. Polarean

Polarean Imaging (USA) is the first company to start manufacturing equipment for obtaining HP gases ¹²⁹Xe and ³He. Polarean offers a set of medical equipment in the form of a hyperpolarizer, a measuring station, a device for inhaling polarized gas, which is a disposable bag with a mouthpiece and a patented drug i.e. gas mixture based on ¹²⁹Xe [83]. However, until the end of 2021 the FDA (Federal Drug Agency) approval for the use of Polarean polarizers in clinical medicine has not yet been received by this company. Therefore, at present, Polarean polarizers are used only by research organizations studying almost all types of lung diseases, including asthma, mucoviscidosis, chronic obstructive pulmonary disease, interstitial lung disease, and more recently — pulmonary vascular disease.

2.2.2.3. Polaris

Scientists and engineers from the POLARIS laboratory (University of Sheffield, United Kingdom) presented a productive unit (up to 3.6 l/h) for obtaining HP ¹²⁹Xe [4,84] (Fig. 24), in the gas mixture of which both xenon of natural composition and enriched (up to 86%) xenon are used. Publications [4,85] studied the ability of ¹²⁹Xe to dissolve in the bloodstream and its sensitivity to chemical shift in the local environment, which makes it possible to monitor gas exchange in the lungs, perfusion of the brain and kidneys, as well as blood oxygen saturation.

2.2.2.4. Micro

Along with the current trend towards increasing the size of the SEOP cell, the first developments relating miniature

SEOP cells [86,87] appeared in the second decade of the 21st century. Such devices are produced by etching holes and grooves in a silicon wafer during the fabrication process, resulting in a series of chambers and channels (Fig. 25). The silicon chip has dimensions 39 × 19 mm at a thickness of 1 mm. The pumping 1 and measuring 2 chambers have dimensions of 4 × 4 mm. The microchannel connecting the pumping and measuring chambers has a length of 10 mm and a width of 1 mm. The outer chambers 3 and 4 serve as places for attaching glass connections to the external gas system and have dimensions of 5 × 10 mm. One side of the wafer is immediately glued with borosilicate glass, and the other one — after applying to the first glass of a RbN₃ microdrop, from which rubidium in the solid state is obtained by photolysis according to the reaction



An ultrasensitive SEOP microplatform is shown, which provides ¹²⁹Xe polarization reaching 7% at pumping power of 1 to 70 mW. The magnetic field for the SEOP process with amplitude of 1 μT was created in *z*-direction by Helmholtz coils (Fig. 25). The microplatform and Helmholtz coils were placed inside a μ-metal screen.

At flow rate of 5 μl/s and the use of gas mixture containing 800 Torr of naturally occurring xenon, the capacity of polarized ¹²⁹Xe is 0.97 μl/(s · W) was reached. Using the same gas mixture under stopped-flow conditions, a spin transfer efficiency of 0.005 was achieved. These results exceed, for example, the 30% polarization of ¹²⁹Xe nuclei, capacity of 0.45 μl/(s · W) of ¹²⁹Xe and spin transfer efficiencies 0.005 obtained on a large-scale SEOP unit [31].

2.2.2.5. North Carolina

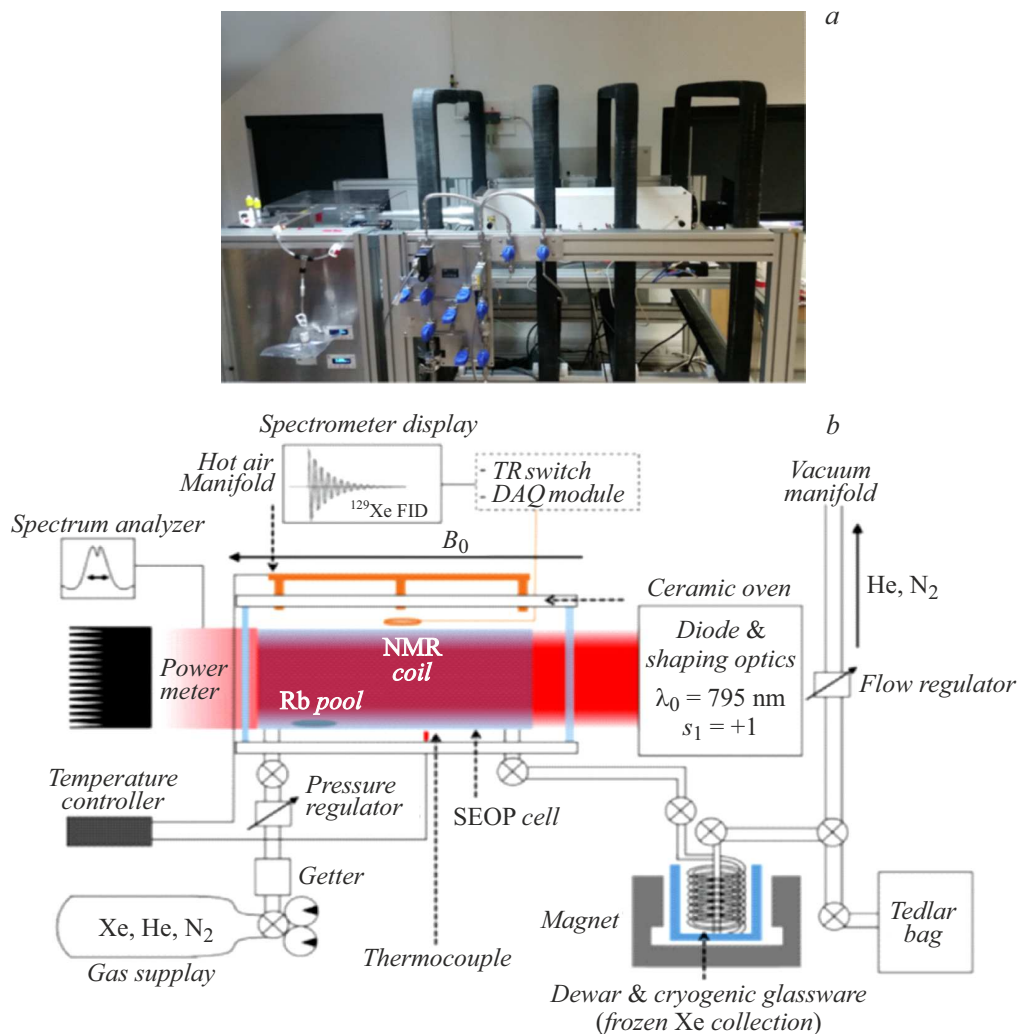


Figure 24. Appearance (a) and schematic design (b) of the Polaris polarizer (adapted from paper [4]).

In the paper [88] the validity of the assumptions usually made regarding the thermodynamic state of Rb vapors inside the optical pumping cell and their gas dynamics is studied by finite element modeling of realistic models of optical pumping cells (using the Polarean 9800 as an example), as well as by optical spectroscopy of cells. It is shown that the final polarization of Xe depends on the Rb density and on the time of Xe presence inside the optical pumping cell. From modeling of three different full size optical cell models it is clear that the time of presence depends on the geometry, not just the gas flow rate and cell volume. By simply changing the location and style of the inlet hole, different time of presence distributions can be obtained for the same cell volume and flow rate. In particular, it can be concluded that more efficient polarizers have longer optical cells.

2.2.2.6. Kioto

In the study [89] an attempt was made to improve the polarizer stability by focusing on the role and properties of the alkali metal used in the SEOP method in the gas mixture

recirculation mode. Rb vapors, which act as a catalyst in the main process of spin transfer from circular polarized photons to noble gas nuclei, are extremely sensitive to moisture or oxygen in the atmosphere, and therefore such catalyst is immediately „poisoned“ as soon as trace amounts of these pollutant gases enter the HP system. Besides, in the recirculating version of the SEOP system a small amount of pollutant gases can be released from the original Rb sample, even if it is pre-cleaned. Therefore, the first prerequisite for the stable operation of the polarizer is to protect the system from contamination. Secondly, the constant pressure of the Rb vapor in the SEOP cell is necessary to ensure the stability of the NMR signal. Therefore, two separate chambers are placed in front of the SEOP cell. The first is the K–Na alloy, which removes gases that react with Rb very effectively as compared to sorbents such as silica gel or zeolite. The second contains metal Rb, which is heated to the same temperature as the SEOP cell and agitated to maintain stable Rb evaporation. These two chambers are located separately from the Helmholtz coils so that the agitators of these chambers do not interfere with the

uniformity of the magnetic field generated by the Helmholtz coils.

2.2.2.7. Mobile 1

The paper [90] presents a mobile unit for SEOP of gas containing ^{129}Xe , the task of which is to produce HP gas offline in close proximity to hospitals or research laboratories. The receiving laboratory must only supply compressed air and mains power. Typical pressures inside the SEOP cell are 0.1 bar of xenon supplemented with

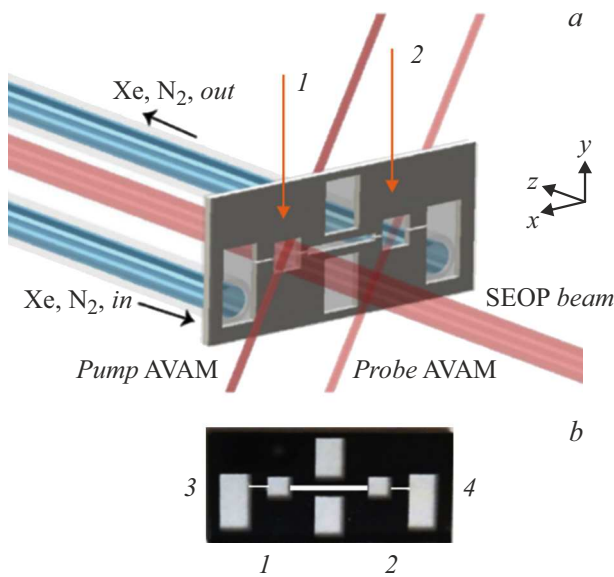


Figure 25. ^{129}Xe polarizer made from silicon wafer. Scheme of operation of the polarizer (a) and the chip (b). Mixture of Xe and N_2 gases flows from the gas manifold to the SEOP microplatform. The laser beam with circular polarization and wavelength of 795 nm optically polarizes the Rb hot vapor in the pumping chamber. When ^{129}Xe passes through it, it is polarized by spin exchange with a polarized vapor of Rb atoms. Additional laser beams with wavelength of 795 nm are used for optical probing of the magnetic field in the pumping and measuring chambers, causing minimum disturbance of the polarization state (measurement of laser power below $100\mu\text{W}$ (adapted from paper [87])).

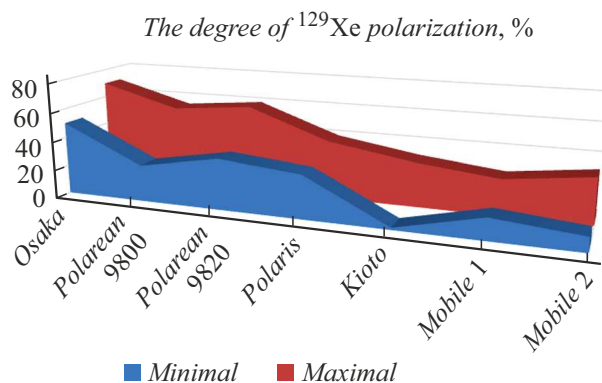


Figure 26. Minimum and maximum degree of polarization of ^{129}Xe nuclear spins at different units.

Total gas flow rates, ml/min

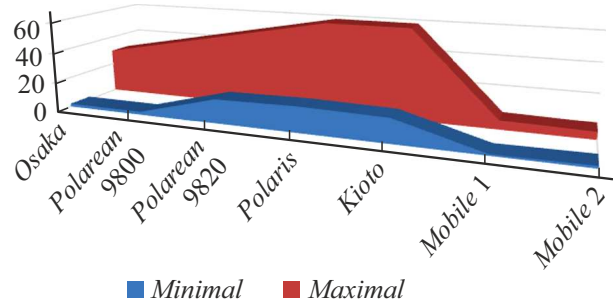


Figure 27. Capacity of polarizers with continuous flow mode.

nitrogen to 0.4 bar and then with helium to 3.5 bar at room temperature. As a rule, the values of the degree of polarization of xenon nuclei are obtained in the range of 0.15 to 0.25%.

2.2.2.8. Mobile 2

An autonomous and portable system for ^{129}Xe polarization by optical pumping with spin exchange with Rb atoms is described in paper [91]. This mobile polarizer can operate in intermittent or continuous flow mode with an average amount of HP ^{129}Xe . The key element is the operational nuclear magnetic resonance module, which facilitates the continuous monitoring of polarization generation in the pumping cell, as well as the calculation of the absolute polarization of ^{129}Xe . In the stopped-flow mode the highest polarization ^{129}Xe $P_{\text{Xe}} = 40\%$ was achieved using xenon partial pressure of 0.1 mbar. In the continuous flow mode with xenon capacity of 6.5 and 26 ml/min, the values $P_{\text{Xe}} = 25$ and 13%, respectively, were achieved.

Detailed information on xenon polarizers with continuous flow is presented in Table 3.

2.2.2.9. Comparison of „continuous flow“ polarizers

It can be seen from the data given in Table 3 that all units are designed for the production of gas mixture containing nuclei of polarized ^{129}Xe at pressures ranging from 1 to 6 bar and temperatures of 70 to 170°C. Variations in the degree of polarization are shown in Fig. 26. Fig. 27 is a diagram that compares „continuous flow“ units in terms of such an important parameter as capacity.

From the information given in Tables 2 and 3, it follows that, due to the applied design and project solutions, each of the units has its own advantages, which for other units appear to be disadvantages. In this regard, when solving the problem of creating ^{129}Xe polarizers, the designers are recommended to take into account the advantages and disadvantages of existing units in order to expand the functionality and stability of parameters that affect the process of production and transfer of HP xenon to users i.e. to testers and clinicians.

Table 3. Free data on the designs of continuous flow polarizers for the period 2011–2021

Design	Power of LDA (W), line width, nm	Polarization of xenon, %	Composition of gas mixtures, partial pressures	Dimensions cell dimensions, process temperature	SEOP magnetic field, mT	NMR frequency	Flow	Magnetic field for cryo-storage, T	Reference
Osaka	90(30 + 60) 2 + 5	50–70	Xe of natural composition: (0.5 to 4.5 kPa), N ₂ or isobutene: 97–70% (14.5 to 10.5 kPa) Mixture: 0.015–0.15 bar	Internal diameter 4 cm, length 17 cm Volume 850 cm ³ 120°C	12 Magnet of leakage field 9.4 T	External spectrometer 110.6 MHz, 9.4 T	Xe: of 2 to 30 ml/min, N ₂ or isobutene: 69–102 ml/min Mixture: 71 to 140 ml/min	no	[82]
Polarean 9800	71 0.39	25–55	1% Xe of natural composition, 10% N ₂ and 89% ⁴ He Mixture: 3–6 bar	Internal diameter 3.8 to 5.4 cm, length 9 to 12.7 cm volume 100, 200 and 300 cm ³ 120–170°C	2.16	25 kHz	Xe: 2–40 ml/min Mixture: to 0.2 l/min	0.2	[46,92]
Polaris	150–200 0.3	30–40	3% Xe of natural composition or ¹²⁹ Xe enriched (86%), 87% ⁴ He, 10% N ₂ . Mixture pressure 0.4 to 2.3 bar	Internal diameter 7.5 cm, length 80 cm. Volume 3530 cm ³ 60–120°C	3.0	External spectrometer 110.6 MHz, 9.4 T 17.65 MHz 1.5 T	Xe: 1–3.6 l/h (16.6–60 ml/min)	0.25	[84,4]
Micro	1–70 mW	to 7	Xe of natural composition or ¹²⁹ Xe enriched (83%) Mixture composition (pressure in bar): 0.27 Xe/0.8 N ₂ 1.07 Xe/1.07 N ₂	4 × 4 × 1 mm Volume 0.016 cm ³ 140°C	0.001	11.6 Hz	Xe: 5 μl/s or 0.3 ml/min	no	[87]
Kioto	60 2	1.5–31	Xe of natural composition Mixture composition 1 Xe/N ₂ : 90/10 Mixture composition 2 Xe/N ₂ : 3/97 Mixture: 0.15 to 1 bar	Internal diameter 5 cm, length 20 cm, Volume 1500 cm ³ 110°C	26	External spectrometer 110.6 MHz, 9.4 T	Xe: 1–6 ml/min Mixture: 30–50 ml/min	no	[89]
Mobile 1	2 × 30	15–25	Xe of natural composition or ¹²⁹ Xe enriched. (83%) 1.33 bar, N ₂ — to 0.53 bar, ⁴ He — to 4.57 bar	Internal diameter 2.2 cm, length 7 cm Volume 100 cm ³ 72–85°C	10	External spectrometer 110.6 MHz,	Xe: 1.6–5 ml/min	0.5	[90]

Table 3 (continued).

Design	Power of LDA (W), line width, nm	Polarization of xenon, %	Composition of gas mixtures, partial pressures	Dimensions cell dimensions, process temperature	SEOP magnetic field, mT	NMR frequency	Flow	Magnetic field for cryo-storage, T	Reference
Mobile 2	50–75 0.5	10–42	Xe natural composition or ^{129}Xe enriched (91%) 0.2–1.4 bar, N_2 0.2 to 2 bar, ^4He Mixture: 3 to 5 bar	Internal diameter 37.6 mm, length 210 mm Volume 950 cm^3 90–175°C	3.6	40 kHz	Xe: 1.6–26 ml/min	no	[91]
Polarean 9820	170 0.2	35–60	1–2% Xe of natural composition or ^{129}Xe enriched (to 83%), 10% N_2 and 89% ^4He Mixture: 6 bar	Internal diameter 8 cm, length 33 cm Volume 1500 cm^3 120–180°C	2.0	23.1 kHz	Xe: 1–3 l/h (16.6–50 ml/min)	0.3	[93,94]

3. Prospects for the use of HP xenon in medicine

The current „gold standard“ of lung assessment is based on spirometry and gas exchange testing, but it does not provide information on various regions of the lung, including the parenchyma — the supporting lung „framework“. Changes in lung function detected by spirometry or gas exchange do not unambiguously correlate with the severity of symptoms and do not reflect the deterioration in the patient's health. This weak relationship is due to the fact that the lungs are a complex organ in which various disorders can be localized, including changes in gas flow (ventilation), blood flow (perfusion) and gas exchange, which impair airway function.

Proton MRI diagnostics of human lungs has always been a difficult task due to low protons density [3,8,95,96]. Other diagnostic methods either use ionizing radiation (computed tomography, positron emission tomography, single photon emission computed tomography) or provide very limited information (spirometry).

Since the first human lung NMR image obtained using HP ^3He [97], most medical researches to date has been performed using this particular contrast agent. For example, the heterogeneous distribution of ventilation has been studied in asthma [98], chronic obstructive pulmonary disease (COPD) [99] and mucoviscidosis [100].

Initial tests conducted to evaluate the safety and tolerability of HP ^{129}Xe inhalation showed that no by-effects were observed during imaging reporting [101,102] although xenon has strong anesthetic properties [2]. Healthy subjects,

as well as patients with mild to moderate COPD, tolerated the inhaled dose of HP ^{129}Xe quite well [103].

The introduction of HP ^{129}Xe opens up new opportunities in human lung MRI, in addition to anatomical, ventilation and perfusion studies. In particular, it is possible to measure the alveolar surface area, septal thickness and vascular transit time (the average time that red blood cells spend within a certain volume of capillary circulation) [103,104], to determine some microstructural changes in an emphysematous lung [27,105,106]. Moreover, the method is sensitive enough to detect lung cancer at a very early stage [7,27].

Lung imaging is becoming critical for diagnosis and treatment methods selection in the face of a huge increase in lung diseases, including the Covid-19 coronavirus pandemic. From early 2021 several publications appeared in which MRI on HP ^{129}Xe was used to study the consequences of coronavirus diseases [107,108]. It was shown that many changes in the lungs and connective tissues are not detected using standard MRI studies, but are clearly distinguishable using MRI on HP xenon.

Hyper-CEST is a new HP ^{129}Xe method developed by the A. Pines group [109]. CEST is a method of saturation transfer with NMR chemical shift that enhances the signal from areas where this NMR biosensor is located [110]. This allows detection of the molecule-target in a non-invasive way. For example, by encapsulating HP ^{129}Xe atoms in cryptophane [111,112], one can detect tissue biomarkers of special interest for biological systems [109,113]. Cryptophane biosensors designed to detect proteins, metal ions, nucleic acids have now reached the limits of detection of such substances in the range of their concentrations from nanomolar to femtomolar [113–115]. Such a high

sensitivity will make it possible to conduct diagnostic studies with tumor markers instead of similar studies with radiopharmaceuticals.

Conclusion

Any MRI or NMR study with HP ^{129}Xe requires access to a source of HP gas. It is safe to say that the growing demand for HP ^{129}Xe will drive further progress in the design of polarizers based on the SEOP method, improving their capacity and providing large volumes of HP gas for various applications.

It can be assumed that for medical diagnostic purposes in the near future it is quite realistic to design mass-produced scanners that will be much cheaper than the current ones. Perhaps the situation will develop similarly to PET tomography centers [116], when one cyclotron serves several scanners in various medical centers, and here one polarizer can serve several MRI scanners and NMR spectrometers [21].

Conflict of interest

The authors declare that they have no conflict of interest.

References

- [1] Prikaz MZ RF 8 oktyabrya 1999 . № 363. O razreshenii meditsinskogo primeneniya lekarstvennykh sredstv (1999). (in Russian) <https://docs.cntd.ru/document/901746690>
- [2] Sbornik metodicheskikh rekomendatsiy (pod obschey redaktsiyey Potapova A.V.) *Primenenie ksenona v klinicheskoy praktike* (NKO ASMG, M., 2019) (in Russian)
- [3] J.P. Hornak. *The Basics of MRI* (Rochester Institute of Technology, Rochester, 1996)
- [4] H. Marshall, N.J. Stewart, Ho-Fung Chan, M. Rao, G. Norquay, J.M. Wild. *Progr. Nucl. Magn. Reson. Spectr.*, **122**, 42 (2021). DOI: 10.1016/j.pnmrs.2020.11.002
- [5] D.A. Barskiy, A.M. Coffey, P. Nikolaou, D.M. Mikhaylov, B.M. Goodson, R. Branca, G.J. Lu, M.G. Shapiro, Ville-Veikko Telkki, V.V. Zhivonitko, I.V. Koptyug, O.G. Salnikov, K.V. Kovtunov, V.I. Bukhtiyarov, M. Rosen, M.J. Barlow, S.S. Safavi, I.P. Hall, L. Schröder, E.V. Chekmenev. *Chem. A Europ. J.*, **23**(4), 725 (2017). DOI: 10.1002/chem.201603884
- [6] B.M. Goodson, N. Whiting, A.M. Coffey, P. Nikolaou, F. Shi, M.E. Gemeinhardt, R.V. Shchepin, J.G. Skinner, J.R. Birchall, M.J. Barlow, E.Y. Chekmenev. *Encyclopedia of Magnetic Resonance*, **4**, 797 (2015). DOI: 10.1002/9780470034590.emrstm1457
- [7] *Hyperpolarized ^{129}Xe Magnetic Resonance: Concepts, Production, Techniques and Applications*, ed. by T. Meersmann, E. Brunner (Cambridge: Royal Society of Chemistry, 2015).
- [8] *MRI of the Lung*, ed. by H.U. Kauczor, M.O. Wielputz (Springer International Publishing AG, 2018), DOI: 10.1007/978-3-319-42617-4
- [9] M.L. Hirsch, N. Kalechofsky, A. Belzer, M. Rosay, J.G. Kempf. *J. Am. Chem. Soc.*, **137**(26), 8428 (2015). DOI: 10.1021/jacs.5b01252
- [10] T.G. Walker, W. Happer. *Rev. Modern Phys.*, **69**, 629 (1997). DOI:10.1103/REVMODPHYS.69.629
- [11] M. Tamski, J. Milani, C. Roussel, J.-Ph. Ansermet. *Phys. Chem. Chem. Phys.*, **22**, 17769 (2020). DOI: 10.1039/d0cp00984a
- [12] K.M. Ward, A.H. Aletras, R.S. Balaban. *J. Magn. Reson.*, **143**(1), 79 (2000). DOI: 10.1006/JMRE.1999.1956
- [13] K.H. Mok, P. Hore. *Methods*, **34**(1), 75 (2004). DOI:10.1016/J.YMETH.2004.03.006
- [14] R.W. Adams, J.A. Aguilar, A.D. Atkinson, M.J. Cowley, P.I. Elliott, S.B. Duckett, G.G. Green, I.G. Khazal, J. López-Serrano, D.C. Williamson. *Science*, **323**, 1708 (2009). DOI:10.1126/science.1168877
- [15] E. Vaneckhaute, S. De Ridder, J.M. Tyburn, J.G. Kempf, F. Taulelle, J.A. Martens, E. Breynaert. *Chem. Phys. Chem.*, **22**(12), 1150 (2021). DOI: 10.1002/cphc.202100360
- [16] J. Brossel, A. Kastler. *Comptes Rendus.*, **229**(23), 1213 (1949).
- [17] A. Kastler. *J. Phys. Radium*, **11**(6), 255 (1950). DOI: 10.1051/jphysrad:01950001106025500
- [18] J. Brossel, A. Kastler, J. Winter. *J. Phys. Radium*, **13**(12), 668 (1952). DOI: 10.1051/jphysrad:019520013012066800
- [19] A. Kastler. *UFN*, **93**(1), 5 (1967) (in Russian) DOI: 10.3367/UFNr.0093.196709b.0005
- [20] E.A. Tagirov. *Foton*. In kn.: *Fizicheskiiy entsiklopedicheskiy slovar / Gl. red. A.M. Prokhorov* (Sov. entsiklopediya, M., 1983) (in Russian) <http://es.niv.ru/doc/dictionary/physical/index.htm>
- [21] G.Yu. Grigoriev, Sh.Sh. Nabiev. *Khimicheskaya fizika*, **37**(5), 3 (2018) (in Russian). DOI: 10.7868/S0207401X18050011
- [22] C.V. Rice, D. Rafferty. *J. Chem. Phys.*, **117**(12), 5632 (2002). DOI: 10.1063/1.1500733
- [23] W. Happer, E. Miron, S. Schaefer, W.A. Van Wijngaarden, X. Zeng. *Phys. Rev. A*, **29**, 3092 (1984). DOI: 10.1103/PHYSREVA.29.3092
- [24] S. Appelt, A. Ben-Amar Baranga, C. Erickson, M.V. Romalis, A.R. Young. *Phys. Rev. A*, **58**(2), 1412 (1998). DOI: 10.1103/PHYSREVA.58.1412
- [25] M. Kelley, R. Branca. *J. Appl. Phys.*, **129**, 154901 (2021). DOI: 10.1063/5.0037440
- [26] T. Walker. *Rev. Modern Phys.*, **69**(2), 629 (1997). DOI: 10.1103/REVMODPHYS.69.629
- [27] *Hyperpolarized and Inert Gas MRI: From Technology to Application in Research and Medicine*, ed. by M.S. Albert, F.T. Hane (Elsevier, Amsterdam, 2017)
- [28] W. Happer. *Rev. Modern Phys.*, **44**, 169 (1972). DOI: 10.1103/RevModPhys.44.169
- [29] W. Happer, Yuan-Yu Jau, T. Walker. *Optically Pumped Atoms*. (WILEY-VCH Verlag GmbH & Co. KGaA, Weinheim, 2010)
- [30] A.L. Zook, B.B. Adhyaru, C.R. Bowers. *J. Magn. Reson.*, **159**(2), 175 (2002). DOI: 10.1016/s1090-7807(02)00030-7.
- [31] P. Nikolaou, A.M. Coffey, L.L. Walkup, B.M. Gust, N. Whiting, H. Newton, S. Barcus, I. Muradyan, M. Dabaghyan, G.D. Moroz, M.S. Rosen, S. Patz, M.J. Barlow, E. Chekmenev, B.M. Goodson. *Proceed. National Academy Sci. (PNAS)*, **110**(35), 14150 (2013). DOI: 10.1073/pnas.1306586110

- [32] A.S. Khan, R.L. Harvey, J.R. Birchall, R.K. Irwin, P. Nikolaou, G. Schrank, K. Emami, A. Dummer, M.J. Barlow, B.M. Goodson, E.Y. Chekmenev. *Angew. Chem. Int. Ed.*, **60**, 22126 (2021). DOI: 10.1002/anie.202015200
- [33] B. Driehuys, G.D. Cates, E. Miron, K. Sauer, D.K. Walter, W. Happer. *Appl. Phys. Lett.*, **69**, 1668 (1996). DOI: 10.1063/1.117022
- [34] U. Ruth, T. Hof, J. Schmidt, D. Fick, H.J. Jänsch. *Appl. Phys. B*, **68**, 93 (1999). DOI: 10.1007/S003400050592
- [35] Elektronik resurs Rezhim dostupa „INZhEKT Rosatom“ Awebdesign Studio, 2020 (in Russian) <https://nppinject.ru/produktsiya/> [Date of access: 31 01 2022].
- [36] A. Zook, C.R. Bowers. *High Capacity Production of > 40% Spin Polarized Xenon-129 for NMR and MRI Applications at the NHMFL*. NHMFL Reports Fall 2001 (NHMFL, Florida State University, 2001)
- [37] V.I. Bakhmutov. *NMR Spectroscopy in Liquids and Solids* (CRC Press, N.Y., 2015), DOI: 10.1201/b18341
- [38] H. Zhu, I.C. Ruset, F.W. Hersman. *Opt. Lett.*, **30** (11), 1342 (2005). DOI: 10.1364/OL.30.001342
- [39] B.L. Volodin, S.V. Dolgy, E.D. Melnik, E. Downs. *Opt. Lett.*, **29** (16), 1891 (2004). DOI: 10.1364/OL.29.001891
- [40] N. Whiting, P. Nikolaou, N.A. Eschmann, M.J. Barlow, R. Lammert, J. Ungar, W. Hu, L. Vaissie, B.M. Goodson. *Appl. Phys. B*, **106** (4), 775 (2012). DOI: 10.1007/S00340-012-4924-X
- [41] P. Siddons, C.S. Adams, C. Ge, G. Hughes. *J. Phys. B. Atom. Mol. Opt. Phys.*, **41** (15), 155004 (2008). DOI: 10.1088/0953-4075/41/15/155004
- [42] A. Banerjee, D. Das, V. Natarajan. *Europhys. Lett.*, **65** (2), 172 (2004). DOI: 10.1209/EPL/I2003-10069-3
- [43] G. Norquay. PhD thesis. *Spin-Exchange Optical Pumping and Nuclear Magnetic Resonance of ¹²⁹Xe*. (Sheffield, United Kingdom: Royal Hallamshire Hospital, 2014)
- [44] J.G. Skinner. PhD thesis. *Optimization of Xenon-Rich Stopped-Flow Spin-Exchange Optical Pumping for Functional Lung Imaging* (Nottingham, University of Nottingham, 2016)
- [45] J.R. Birchall, R.K. Irwin, P. Nikolaou, A.M. Coffey, B.E. Kidd, M. Murphy, M. Molway, L.B. Bales, K. Ranta, M. Barlow, B.M. Goodson, M. Rosen, E. Chekmenev. *J. Magn. Res.*, **319**, 106813 (2020). DOI: 10.1016/j.jmr.2020.106813
- [46] M.S. Freeman. PhD thesis. *The Efficiency Limits of Spin Exchange Optical Pumping Methods of ¹²⁹Xe Hyperpolarization: Implications for in vivo MRI Applications* (Duke University, Durham, 2015)
- [47] B.C. Anger, G. Schrank, A. Schoeck, K.A. Butle, M.S. Solu, R.J. Pugmire, B. Saam. *Phys. Rev. A*, **78**, 043406 (2008). DOI: 10.1103/PhysRevA.78.043406
- [48] S. Breeze, S. Lang, I. Moudrakovski, C. Ratclif. *J. Appl. Phys.*, **87**, 8013 (2000). DOI: 10.1063/1.373489
- [49] T. Pałasz, L. Mikowska, B. Głowacz, Z. Olejniczak, M. Suchanek, T. Dohnalik. *Acta Phys. Polonica A*, **136** (6), 1008 (2019). DOI: 10.12693/APhysPolA.136.1008
- [50] L. Repetto, S. Zimmer, F. Allmendinger, P. Blümler, M. Doll, J.O. Grasdijk, W. Heil, K. Jungmann, S. Karpuk, H. Krause, A. Offenhäusser, U. Schmidt, Y. Sobolev, L. Willmann. *J. Magn. Res.*, **265**, 197 (2016). DOI: 10.1016/j.jmr.2016.02.011
- [51] N.N. Kuzma, B. Patton, K. Raman, W. Happer. *Phys. Rev. Lett.*, **88** (14), 147602 (2002). DOI: 10.1103/PHYSREVLETT.88.147602
- [52] M. Repetto, P. Blümler, W. Heil, S. Karpuk, K. Tullney, E. Babcock. *J. Magn. Res.*, **252**, 187 (2015). DOI: 10.1016/j.jmr.2015.01.015
- [53] E.G. Sorte, B.V. Fine, B. Saam. *Phys. Rev. B*, **85** (17), 174425 (2012). DOI: 10.1103/PhysRevB.85.174425
- [54] M.S. Rosen, T.E. Chupp, K.P. Coulter, R.C. Welsh, S.D. Swanson. *Rev. Scien. Instrum.*, **70** (2), 1546 (1999). DOI: 10.1063/1.1149622
- [55] N.J. Shah, T. Unlu, H.P. Wegener, H. Halling, R. Zilles, S. Appelt. *NMR in Biomedicine*, **13** (4), 214 (2000). DOI: 10.1002/1099-1492(200006)13:4<214::AID-NBM634>3.0.CO;2-G
- [56] J.C. Leawoods, B.T. Saam, M.S. Conradi. *Chem. Phys. Lett.*, **327**, 359 (2000). DOI: 10.1016/S0009-2614(00)00908-8
- [57] L.J. Smith, J. Smith, E. MacNamara, K. Knagge, D. Raftery. *J. Phys. Chem. B*, **105**, 1412 (2001). DOI: 10.1021/JP0032309
- [58] C.V. Rice, D. Raftery. *J. Chem. Phys.*, **117** (12), 5632 (2002). DOI: 10.1063/1.1500733
- [59] A. Wakai, J. Kershow, K. Nakamura, H. Iida, H. Tamura, Y. Kondon, I. Kanno. *Magn. Res. Med. Sci.*, **2** (4), 189 (2003). DOI: 10.1002/1099-1492(200006)13:4<220::AID-NBM638>3.0.CO;2-F
- [60] B. Driehuys, J. Pollaro, G.P. Cofer. *Magn. Res. Med.*, **60** (1), 14 (2008). DOI: 10.1002/mrm.21651
- [61] H. Imai, J. Fukutomi, A. Kimura, H. Fujiwara. *Concepts in Magnetic Resonance Part B: Magn. Res. Engineer.*, **33**, 192 (2008). DOI: 10.1002/CMR.B.20117
- [62] S. Appelt, F.W. Hasing, H. Kuhn, J. Perlo, B. Blumich. *Phys. Rev. Lett.*, **94**, 197602 (2005). DOI: 10.1103/PHYSREVLETT.94.197602
- [63] X.J. Chen, H.E. Moller, M.S. Chawla, G.P. Cofer, B. Driehuys, L.W. Hedlund, G.A. Johnson. *Magn. Res. Med.*, **42**, 721 (1999). DOI: 10.1002/(SICI)1522-2594(199910)42:4<729::AID-MRM15>3.0.CO;2-2
- [64] S. Appelt, T. Unlu, K. Zilles, N.J. Shah, S. Baer-Lang, H. Halling. *Appl. Phys. Lett.*, **75** (3), 427 (1999). DOI: 10.1063/1.124397
- [65] R. Seydoux, A. Pines, M. Haake, J.A. Reimer. *J. Phys. Chem. B*, **103** (22), 4629 (1999). DOI: 10.1021/JP9821984
- [66] K. Ruppert, J.R. Brookeman, K.D. Hagspiel, B. Driehuys, J.P. Mugler III. *NMR in Biomedicine*, **13**, 220 (2000). DOI: 10.1002/1099-1492(200006)13:4<220::AID-NBM638>3.0.CO;2-F
- [67] K. Ruppert, J.R. Brookeman, K.D. Hagspiel, J.P. Mugler III. *Magn. Res. Med.*, **44**, 349 (2000). DOI: 10.1002/1522-2594(200009)44:3<349::AID-MRM2>3.0.CO;2-J
- [68] T. Meersmann, J.W. Logan, R. Simonutti, S. Caldarelli, A. Comotti, P. Sozzani, L. Kaiser, A. Pines. *J. Phys. Chem. A*, **104** (50), 11665 (2000). DOI: 10.1021/JP002322V
- [69] F.W. Hersman, L.C. Ruset, S. Ketel, I. Muradian, S. Covrig, J. Distelbrink, W. Porter, D. Watt, J. Ketel, J. Brackett, A. Hope, S. Patz. *Acad. Radiol.*, **15** (6), 683 (2008). DOI: 10.1016/j.acra.2007.09.020
- [70] A. Asfour. *J. Biomed. Sci. Engineer.*, **03**, 1099 (2010). DOI: 10.4236/JPB.2010.311143
- [71] P. Nikolaou, N. Whiting, N.A. Eschmann, K. Chaffee, B.M. Goodson, M. Barlow. *J. Magn. Res.*, **197** (2), 249 (2009). DOI: 10.1016/j.jmr.2008.12.015

- [72] Z.I. Cleveland, H.E. Müller, L.W. Hedlund, B. Driehuys. *J. Phys. Chem. B*, **113** (37), 12489 (2009). DOI: 10.1021/jp9049582
- [73] G. Schrank, Z. Ma, A. Schoeck, B. Saam. *Phys. Rev. A*, **80**, 063424 (2009). DOI: 10.1103/PHYSREVA.80.063424
- [74] J.S. Six, T. Hughes-Riley, K.F. Stupic, G.E. Pavlovskaya, T. Meersmann. *Public Library of Science one (PLOS 1)*, **7**(11), e49927 (2012). DOI: 10.1371/journal.pone.004992
- [75] P. Nikolaou, A.M. Coffey, L.L. Walkup, B.M. Gust, C.D. La Pierre, E. Koehnemann, M.J. Barlow, M.S. Rosen, B.M. Goodson, E.Y. Chekmenev. *J. Am. Chem. Soc.*, **136** (4), 1636 (2014). DOI: 10.1021/ja412093d
- [76] J.R. Birchall, R.K. Irwin, M.R.H. Chowdhury, P. Nikolaou, B.M. Goodson, M.J. Barlow, A. Shcherbakov, E.Y. Chekmenev. *Anal. Chem.*, **93** (8), 3883 (2021). DOI: 10.1021/acs.analchem.0c04545
- [77] J.R. Birchall, P. Nikolaou, A.M. Coffey, B.E. Kidd, M. Murphy, M. Molway, L.B. Bales, B. Goodson, R.K. Irwin, M.J. Barlow, E.Y. Chekmenev. *Anal. Chem.*, **92** (6), 4309 (2020). DOI: 10.1021/acs.analchem.9b05051
- [78] P. Nikolaou, A.M. Coffey, M.J. Barlow, M.S. Rosen, B.M. Goodson, E.Y. Chekmenev. *Analyt. Chem.*, **86** (16), 8206 (2014). DOI: 10.1021/ac501537w
- [79] P. Nikolaou, A.M. Coffey, L.L. Walkup, M. Gust, N. Whiting, H. Newton, I. Muradyan, M. Dabaghyan, K. Ranta, G.D. Moroz, M. Rosen, S. Patz, M. Barlow, E. Chekmenev, B.M. Goodson. *Magn. Res. Imag.*, **32** (5), 541 (2014). DOI: 10.1016/j.mri.2014.02.002
- [80] W.T. Lee, G. Zheng, C.L. Talbot, X. Tong, T. D'Adam, S. Parnell, M. de Veer, G.R. Polglase, S.B. Hooper, B.R. Thompson, F. Thien, G.F. Egan. *Magn. Res. Imag.*, **79**, 112 (2021). DOI: 10.1016/j.mri.2021.02.010
- [81] J. Skinner, K. Ranta, A.M. Coffey, P. Nikolaou, M.S. Rosen, E.Y. Chekmenev, P.G. Morris, M.J. Barlow, B.M. Goodson. *J. Magn. Res.*, **312**, 06686 (2020). DOI: 10.1016/j.jmr.2020.106686
- [82] H. Imai, H. Yoshimura, A. Kimura, H. Fujiwara. *Scientific Reports*, **7** (1), 7352 (2017). DOI: 10.1038/s41598-017-07695-7
- [83] *Hyperpolarized Gas MRI for Pulmonary Disease Assessment: Interview with Richard Hullihen, CEO of Polarean Imaging.* <https://www.medgadget.com/2020/09/hyperpolarized-gas-mri-for-pulmonary-disease-assessment.html>. [Date of access: 29.12.2021].
- [84] G. Norquay, G.J. Collier, M. Rao, N.J. Stewart, J.M. Wild. *Phys. Rev. Lett.*, **121**, 153201 (2018). DOI: 10.1103/PhysRevLett.121.153201
- [85] M. Rao, N.J. Stewart, G. Norquay, P.D. Griffiths, J.M. Wild. *Magn. Res. Med.*, **75** (6), 2227 (2016). DOI: 10.1002/mrm.26241
- [86] R. Jimenez-Martinez, D.J. Kennedy, M. Rosenbluh, E. Donley, S. Knappe, S.J. Seltzer, H.L. Ring, V. Bajaj, J. Kitching. *Nature Commun.*, **5**, 3905 (2014). DOI: 10.1038/ncomms4908
- [87] D.J. Kennedy, S. Seltzer, R. Jiménez-Martínez, H.L. Ring, N.S. Malecek, S. Knappe, E. Donley, J. Kitching, V. Bajaj, A. Pines. *Nature Sci. Reports*, **7**, 43994 (2017). DOI: 10.1038/srep43994
- [88] M. Kelley, A. Burant, R.T. Branca. *J. Appl. Phys.*, **128**, 144901 (2020). DOI: 10.1063/5.0019074
- [89] H. Fujiwara, H. Imai, A. Kimura. *Analytical Sci.: Intern. J. Jpn. Society Analyt. Chem.*, **35**, 869 (2019). DOI: 10.2116/analsci.19P047
- [90] C. Chauvin, L. Liagre, C. Boutin, E. Mari, E. Léonce, G. Carret, B. Coltrinari, P. Berthault. *Rev. Sci. Instrum.*, **87**, 016105 (2016). DOI: 10.1063/1.4940928
- [91] S.E. Korchak, W. Kilian, L. Mitschang. *Appl. Magn. Res.*, **44**, 65 (2013). DOI: 10.1007/s00723-012-0425-7
- [92] M.S. Freeman, K. Emami, B. Driehuys. *Phys. Rev. A, Atomic, Molec., Opt. Phys.*, **90**, 023406 (2014). DOI: 10.1103/PHYSREVA.90.023406
- [93] *Xenon MRI Platform.* <https://polarean.com/xenon-mri-platform/#hyperpolarizer>. [Date of access: 28.12.2021].
- [94] J.W. Plummer, K. Emami, A. Dummer, J.C. Woods, L.L. Walkup, Z.I. Cleveland. *J. Magn. Res.*, **320**, 106845 (2020). DOI: 10.1016/j.jmr.2020.106845
- [95] J.M. Wild, H. Marshall, M. Bock, P.M. Jakob, M. Puderbach, F. Molinari, E.J. Van Beek, J. Biederer. *Insights Imag.*, **3**, 345 (2012). DOI: 10.1007/s13244-012-0176-x
- [96] R. Freeman, R. Smith. *Magnetic Resonance in Chemistry and Medicine.* (Oxford University Press, Oxford, 2003)
- [97] H.U. Kauczor, D. Hofmann, K. Kreitner, H. Nilgens, R. Surkau, W. Weil, A. Potthast, M.V. Knopp, E.W. Otten, M. Thelen. *Radiology*, **201** (2), 564 (1996). DOI: 10.1148/radiology.201.2.8888259
- [98] R. Aysola, E.E. de Lange, M. Castro, T. Altes. *J. Magn. Res. Imag.*, **32**, 1379 (2010). DOI: 10.1002/jmri.22388
- [99] A.J. Swift, J.M. Wild, S. Fischele, N. Woodhouse, S. Fleming, J. Waterhouse, R. Lawson, M. Paley, E.J. Van Beek. *Europ. J. Radiology*, **54** (3), 352 (2005). DOI: 10.1016/J.EJRAD.2004.08.002
- [100] L. Donnelly, J.R. MacFall, H.P. McAdams, J.M. Majura, J. Smith, D.P. Frush, P. Bogonad, H. Charles, C.E. Ravin. *Radiology*, **212** (3), 885 (1999). DOI: 10.1148/RADIOLOGY.212.3.R99SE20885
- [101] F. Hersman, J. Ketel, I. Ruset, S. Ketel, I. Dregely, W. Porter, D. Watt, J. Mugler, T. Altes, K. Ruppert, J. Mata, S. Patz, H. Hatabu, M. Hrovat, I. Muradian, M. Dabaghyan, G. Miller, C. Wang, J. Butler, J. Distalbrin. *Proc. Intl. Soc. Mag. Reson. Med.*, **18** (6), 4598 (2010).
- [102] B. Driehuys, S. Martinez-Jimenez, Z. Cleveland, G.M. Metz, D.M. Beaver, J.C. Nouls, S.S. Kaushik, R. Firszt, C. Willis, K.T. Kelly, J. Wolber, M. Kraft, P. McAdams. *Radiology*, **262** (1), 279 (2012). DOI: 10.1148/radiol.11102172.
- [103] A. Fitterman. *Theory and Production of Hyperpolarized Xenon Gas for Lung and Brain* (Lakehead University, Orillia, Ontario, 2015)
- [104] B. Driehuys, G.P. Cofer, J. Pollaro, J.B. Mackel, L.W. Hedlund, G.A. Johnson. *Proc. Natl. Acad. Sci. (PNAS)*, **103** (48), 18278 (2006). DOI: 10.1073/pnas.0608458103
- [105] B. Saam, D. Yablonskiy, V. Kodibagkar, J. Leawoods, J.D. Gierada, J. Cooper, S. Lefrak, M. Conradi. *Magn. Reson. Med.*, **44**, 174 (2000). DOI: 10.1002/1522-2594(200008)44:2;174::aid-mrm2;3.0.co;2-4
- [106] S.S. Kaushik, Z.I. Cleveland, G.P. Cofer, G. Metz, D. Beaver, J. Nouls, M. Kraft, W. Auermann, J. Wolber, H.P. McAdams, D. Driehuys. *Magn. Res. Med.*, **65** (4), 1155 (2011). DOI: 10.1002/mrm.22697
- [107] J. Grist, M. Chen, G.J. Collier, B. Raman, G. Abu Eid, A. McIntyre, V. Matthews, E. Fraser, Ling-Pei Ho, J.M. Wild, F. Gleeson. *Radiology*, **301** (1), E353 (2021). DOI: 10.1148/radiol.2021210033

- [108] H. Li, X. Zhao, Y. Wang, X. Lou, Sh. Chen, H. Deng, L. Shi, J. Xie, D. Tang, J. Zhao, L. Bouchard, L. Xia, X. Zhou. *Sci. Adv.*, **7** (1), eabc8180 (2021). DOI: 10.1126/sciadv.abc8180
- [109] L. Schroder, T.J. Lowery, C. Hilty, D.E. Wemmer, A. Pines. *Science*, **314** (5798), 446 (2006). DOI: 10.1126/science.1131847
- [110] *Chemical Exchange Saturation Transfer Imaging: Advances and Applications*, ed. by M. Mc Mahon, A.A. Gilad, J.W. Bulte, P.C. van Zijl (Pan Stanford Publishing Pte. Ltd, Singapore, 2017), DOI: 10.1201/9781315364421
- [111] M. Luhmer, B.M. Goodson, Y.-Q. Song, D.D. Laws, L. Kaiser, M.C. Cyrier, A. Pines. *J. American Chem. Society*, **121** (24), 3502 (1998). DOI: 10.1021/JA9841916
- [112] M. Kunth, C. Witte, L. Schröder. *J. Chem. Phys.*, **141** (19), 194202 (2014). DOI: 10.1063/1.4901429
- [113] M. Kunth, C. Witte, L. Schröder. *Pharmaceuticals*, **14**, 79 (2021). DOI: 10.3390/ph14020079
- [114] S.D. Zemerov, I. Dmochowski. *Royal Society Chem. Adv.*, **11** (13), 7693 (2021). DOI: 10.1039/D0RA10765D
- [115] J. Jayapaul, L. Schroder. *Contrast Media Molecular Imag.*, **2019**, 9498173 (2019). DOI: 10.1155/2019/9498173
- [116] *Positron Emission Tomography*, ed. by A. Granov, L. Tiutin, T. Schwarz (Springer- Verlag, Berlin, Heidelberg, 2013), DOI: 10.1007/978-3-642-21120-1.